國立交通大學

光電工程研究所

博士論文

應用於提升表面型微加工的光學讀寫頭功能之微光學次系統

Micro-optical Subsystems for Enhancing the Function of a Surface Micro-machined Optical Pickup

研究生：李企桓

指導教授：謝漢萍 教授

中華民國九十六年九月

應用於提升表面型微加工的光學讀寫頭功能之微光學次系統

Micro-optical Subsystems for Enhancing the Function of a Surface Micro-machined Optical Pickup

研 究 生: 李企桓　　Student: Chi-hung Lee
指導教授: 謝漢萍　　Advisor: Dr. Han-Ping D. Shieh

國立交通大學　電機資訊學院
光電工程研究所
博士論文

A Thesis
Submitted to Department of Photonics & Institute of Electro-Optical Engineering
College of Electrical Engineering and Computer Science
National Chiao-Tung University
in Partial Fulfillment of the Requirements for the Degree of Philosophy In Electro-Optical Engineering
September 2007
Hsin-Chu, Taiwan, Republic of China.

中華民國九十六年九月

應用於提升表面型微加工的光學讀寫頭功能之微光學次系統

研究生：李企桓　　　指導教授：謝漢萍 教授

國立交通大學光電工程研究所

摘要

隨著數位資訊時代的來臨與網際網路的普及，消費性電子產品不斷朝向可攜式化、輕薄短小化、省電、低功率輸出的方向前進。利用微機電製程技術來設計與製作相容於現今光學讀寫系統的光學元件具有體積小、重量輕及適合於批次製造的優點。而自由空間型將所有元件同時製作在一晶片上，具有在設計光罩時即完成光學元件間的對準工作的優點。然而自由空間型仍面臨許多問題，諸如多晶矽製作的光學元件僅可應用於使用近紅外光(780 nm)的CD碟片，無法應用於使用650 nm的DVD碟片及405 nm的HD-DVD碟片，而單光束讀寫碟片及分光鏡效率偏低更嚴重限制其功能。為了改善這些問題，本論文提出了以在可見光波段具有高穿透性的低應力氮化矽取代原先的多晶矽，並結合光柵與微型致動器設計出一可切換式光柵，其可發展成一可切換單/多光束的微型光學讀寫頭。此外，利用多層光學膜的原理，我們製作出可應用於微型光學讀寫頭的高效率極化分光器，以讓自由空間型的微型光學讀寫頭被更廣泛且成功地應用在光儲存領域。為進一步發展出CD/DVD/HD-DVD光碟相容的微型讀寫頭，本論文提出一種二維的微型反射系統，此系統的概念可用於驗證相容型的微型讀寫頭的可行性。

傳統上，具備可切換單/多光束功能的光學讀寫頭是以電壓控制的液晶元件或以一磁控致動器來移動多光束光柵以切換單光束寫入及多光束讀取的狀態。然此二種方式均導致讀寫頭的體積及成本大幅提高。而本論文則成功開發出「微型可切

換式多光束光柵」，完全可由微機電製程製作出，除具備體積小，成本低之優點外，控制簡易。此可切換式多光束光柵是由一微型抬升臂致動器及一多光束相位光柵所組成。

而極化分光器在光學讀寫頭上主要是用來將光分成兩個極化方向互相正交的光束。並搭配四分之一波片，可同時提高去光路的穿透光效率與反射光光效率。一般的極化分光器主要是利用大體積的雙折射晶體或高成本的鍍膜玻璃來製作，均不適合整合於微型光學讀寫頭。本論文所成功開發出「微型高效率極化分光器」，利用多層膜光學的原理，我們將空氣層與低應力氮化矽薄膜層堆疊，建構出在可見光區段具有低損耗及高極化分光效率之極化分光器。

第三種元件為一種二維的反射系統，其包括一拋物形反射面鏡及一菱鏡。其中拋物形反射面鏡係在單晶矽層中蝕刻出一拋物形溝槽(trench)而成，可將經拋物面焦點的入射光以平行拋物面光軸方向反射出或將平行拋物面光軸方向的入射光反射且經拋物面焦點而出。菱鏡為一 Porro(45°-90°-45°)型，主要是將入射光以平行原入射方向反射出，且入射位置與出射位置間存在一位移。藉由適當組合拋物形反射面鏡與菱鏡的位置，可使入射光以特定反射角度反射出。最大掃描角度可達傳統二維的反射面鏡的三至四倍以上，掃描時光以垂直角度進出波導，故掃描角度不因 Snell’s law 而縮減，光繞射損失低，反射中心於掃描期間無偏移現象。

本論文中展現了以微機電技術所製作的微型光學元件於光儲存產業的重大應用潛力，且結合微光學設計與微光機電製程的微型光學系統技術，也將在未來高科技產業中具有益形重要的地位。

Micro-optical Subsystems for Enhancing the Function of a Surface Micro-machined Optical Pickup

Student：Chi-hung Lee Advisor：Dr. Han-Ping D. Shieh

Institute of Electro-Optical Engineering

National Chiao Tung University

Abstract

In the era of multimedia, internet and mobile communication, features of portable , thin, light weight and power saving are required for consuming electronic products. Compared with conventional optical pickup systems, micromachinical optical pickup systems are smaller, lighter and can be made by a batch-fabrication technology.

Among the proposed micro optical pickups, the free-space polysilicon optical bench has been realized on a single chip, on which all the optical elements can be precisely prealigned during the mask design stage. However, this device used thin-polysilicon films as optical patterns and suffered from absorption of visible light by polysilicon. Another challenge in this device was that only a single beam was used by the micro-optical pickup to read and write a disc. Moreover, the beam splitter in the device was of low efficiency. These seriously limit its performance.

In this thesis, to overcome the above issues, a transparent material for visible light was derived from low stress silicon nitride and improved the light efficiency. Besides, two novel components, a switchable grating and a high efficiency polarized beam splitter, were designed to further enhance the performance of the free-space optical pickup.

Conventionally, the switching function can be realized by using a voltage-controlled liquid crystal grating or a magnet-actuated glass grating. The two approaches still suffer from the difficult assembly of optical components of large size and high cost. Therefore, we propose “a micro switchable grating,” which is composed of a stress-induced curved micro actuator and a phase-type grating on the tip of the actuator.

In an optical pickup, a polarized beam splitter (PBS) is used with a quarter-wave plate to improve the transmittance of the forward polarized light and the reflectance of the backward polarized light. Conventionally, the PBS is realized using a birefringence crystal or a films-coated glass. The former is large in size, while the latter is of high cost. Therefore, a micro PBS consisting of a novel stack of two silicon nitride layers separated by an air gap was developed in our research to possess the same function.

Besides, a planar micro-reflective system composed of a parabolic mirror, a prism, and a thermal actuator was demonstrated to verify the feasibility of a CD/DVD/HD-DVD compatible micro-pickup. A mechanical scan angle of 38 degrees was demonstrated by applying the developed planar reflective system, which displayed more than three times the scan angle compared to that of a conventional rotary mirror. The optical simulation about the deflected beam deviating from the optical axis of the planar reflective system was also presented, and good agreement between theory and experiment is achieved.

This dissertation has successfully demonstrated the great potentials of the micro switchable grating, the micro PBS, and the micro-reflective system. These sub-systems

can be achieved using the surface micromachining, potentially also at very low cost. The size of them is also dramatically reduced. Further, the fabrication of these subsystems is compatible with other micro diffractive elements. This makes them feasible to build a multi-function micro-optical pickup for short wavelength optical storage applications in the near future.

致謝

首先感謝指導教授謝漢萍老師在研究、表達能力上對我的指導，使我成長許多。其次要感謝邱一老師及 UC Berkeley 的吳名強老師在這段期間對我的協助與指導。此外，我要感謝原精密儀器中心光學小組的林暉雄學長及田仲豪學長在理論及量測方面的鼎力協助，另外還有交大奈米中心的實驗設備支援。

在此我更要特別感謝各口試委員對本論文所提出的寶貴意見及以下先進的授課，使我獲益良多:

成大工科李國賓老師及其所開授的微致動器設計及微感測器設計兩門課。

清大工科曾繁根老師及其所開授的高等微機電製程實驗。

中央光電李正中老師及其所開授的干涉光學課程及其大作薄膜光學。

中央光電孫文信老師及其所開授的光學系統設計及光學設計專利分析兩門課。

Table of Contents

Abstract (Chinese) i

Abstract (English) iii

Acknowledgments vi

Table of Contents vii

Figure Caption x

List of Tables xiv

Chapter 1 Introduction 1

1.1 Introduction of a micro-optical pickup 1

1.2 Introduction of surface micromachining 3

1.3 Motivation and objective of this thesis 8

1.4 Organization of this thesis 10

Chapter 2 Principle of Microoptics and Micro actuators 12

2.1 Overview of the switchable grating based micro optical pickup 12

2.2 Micro-hinges 15

2.3 Binary phase micrograting 17

2.4 Stress-induced micro-actuator 22

2.5 Summary 26

Chapter 3 Fabrication and Measurement of Switchable Grating 28

3.1 Overview of fabrication process 28

3.2 Release and anti-stiction process 31

3.3 Realization of switchable grating 33

3.4 Experimental results and discussions 35

3.5 Comparisons 38

3.6 Summary 39

Chapter 4 Polarization Beam Splitter 40

4.1 Transmittance, reflectance, and absorptance 41

4.2 2 x 2 matrix formulation for a thin film 44

4.3 Simulation 47

4.4 Silicon nitride film for 405 nm 50

4.5 Summary 53

Chapter 5 Fabrication and Measurement of a Polarization Beam Splitter 54

5.1 Structure design and device fabrication 54

5.2 Experimental results and Discussions 58

5.3 Comparisons 62

5.4 Summary 62

Chapter 6 Micro Reflective System 63

6.1 Optical design 64

6.2 Fabrication 67

6.3 Experimental results and Discussions 68

6.4 Summary 71

Chapter 7 Conclusions and Future Works 73

7.1 Conclusions 73

7.2 Future works 76

Reference 82

Publication list 86

Vita 88

Figure Caption

Fig.1-1 Schematic of a conventional optical pickup 2

Fig.1-2 Schematic of the integrated optic disk pickup (IODPU) 3

Fig. 1-3 Side view of the planar optical disk pickup 5

Fig. 1-4 Schematic of the silicon-based stacked optical pickup 6

Fig. 1-5 Schematic of a free-space micro-optical pickup on a chip 7

Fig. 1-6. Varities of silicon based surface micromaching 8

Fig. 2-1. Schematic of the micro-optical pickup with a switchable grating 14

Fig. 2-2. There are four hinge types 16

Fig. 2-3. The phase profile comparison between an ideal sawtooh thickness profile 18

Fig. 2-4. Optical path of the three beams for reading 19

Fig. 2-5. Diffraction ratio ($I_0/I_{\pm1}$) contours 21

Fig. 2-6. Schematic of microactuators commonly used in surface-micromachined optical systems 24

Fig. 2-7. Schematic of dimensions of the polysilicon-gold composite Cantilever 25

Fig. 2-8. Layout of the proposed switchable grating mounted at the end of a bimorph actuator 26

Fig. 3-1. Cross sectional view showing all 7 layers of the surface micromachining process 30

Fig. 3-2. Schematic of the home made release instrument including a 40 watt lamp and a set of Teflone tools 32

Fig. 3-3. Process flow for the dynamic grating 34

Fig. 3-4. SEM of a (a) dynamic grating and (b) micro optical elements in a optical pickup 35

Fig. 3-5. Static lift heights of the free end versus dc bias driving voltages 36
Fig. 3-6. Diffraction patterns versus voltage to the actuator 37
Fig. 3-7. Schematic of a cascaded grating array to produce seven diffraction beams of equal intensity 39
Fig. 4-1. A thin homogenous layer of dielectric material 42
Fig. 4-2 A thin layer of dielectric material 44
Fig. 4-3. Propagation of an electromagnetic wave through a stack of films of thickness d_i and refractive index N_i 47
Fig. 4-4. Calculated reflectivity to transmissivity ratio of the TE mode as a function of d_2 and d_3 at the Brewster angle incidence 49
Fig. 4-5. Dependence of (a) residual stress and (b) complex refractive index, n + ik, on the reaction gas ratio for various annealing times 52
Fig. 5-1. Schematic drawing of the micro PBS: (a) cross-sectional and (b) top view 54
Fig. 5-2. Cross section of the processing sequence for fabricating the micro PBS 56
Fig. 5-3. SEM photographs of (a) the micro pop-up PBS and (b) a micro optical pickup, including a cylindrical lens, a grating, a PBS a folded mirror and an astigmatic lens 57
Fig. 5-4. Configuration of the measurement system 58
Fig. 5-5. Schematic of the cross view of the beam splitter 59
Fig. 5-6. (a) Beam profiles of TE mode before (left) and after (right) reflecting from the micro-PBS. (b) Beam profiles of TM mode before (left) and after (right) transmitting through the micro PBS 60
Fig. 6-1. Schematic of a CD/DVD/HD-DVD compatible micro-optical pickup, which uses a rotary actuated mirror to switch between each light source 63
Fig. 6-2. Schematic of the proposed planar microreflective device, which is composed of a parabolic mirror, a prism, and a thermal actuator 65

Fig. 6-3. (a) The incident angle, θ, is a function of position of point A and the focal length, f. (b) For an incident beam enters a Porro prism, the displacement, S, is related to the entrance point A 65

Fig. 6-4. Schematics of (a) small reflection angle produced by small displacement of the prism and (b) large reflection angle produced by large displacement of the prism 66

Fig. 6-5. Process flow for the planar micro-reflective device 67

Fig.6-6. SEM image of the fabricated PRS (a) The entire PRS including the waveguide to guide the incident light. (b) The enlarged view of the prism and the parabolic reflector 68

Fig. 6-7. Experimental setup for the optical measurement of the PRS 69

Fig. 6-8. The infrared near field images of the optical beams at (a) the front end of the rectangular waveguide, which is the input spot; and (b) the facet of the chip, which is the output spot 70

Fig. 6-9. The reflection angle as a function of prism displacement 70

Fig. 6-10. Schematic of the light reentering the silicon slab 71

Fig. 6-11. Schematic of a CD/DVD/HD-DVD compatible micro-optical pickup, which uses a surface micro-machined linear actuated mirror and a vertical parabolic reflector to switch between each light source 72

Fig 7-1. A surface-micromachined optical pickup based on the finite conjugate design (a) and its specification according to ZEMAX (b) 78

Fig 7-2. FEM shows the deformation of the beam splitter is below $5.6e^{-3}$ 79

Fig 7-3. Photograph of the smart mask design. The etch holes concentrate on the side latches 79

Fig 7-4. Photograph of the 4-phase levels HOE 80

Fig 7-5. Simulation result of focus error signal 80

Fig 7-6. A surface-micromachined optical pickup based on the finite conjugate design 81

List of Tables

Table 1-1 Pros and cons of four micro optic pickup heads 11

Table 3-1: Thickness of each layer in polysilicon-silicon nitride process 31

Table 3-2: Comparison of liquid crystal and stress-induced switchable gratings 39

Table 5-2: Comparison of planar and pop-up polarization beam splitters 61

Table 5-1. Optical performance of the pop-up micro PBS at Brewster angle incidence 6 2

Chapter 1

Introduction

The growth of optical data storage industries has been driven over the last decade by the personal computer revolution. Over the next decade, it is expected to expand even faster, fueled by the internet specific applications and multimedia revolution, particularly for high definition television recording which requires a data-transfer rate of more than 100 Mbps. Following this trend, the storage capacity, data transfer rate, access time, and cost characterize the development of optical disc systems. Among the components in an optical data storage system, the optical pickup plays a key role. A conventional optical pickup is composed of discrete components, whose optical performance is limited by the accuracy of manual assembly. Meanwhile, the weight and large volume hinder its further application as well. Using micro-machining, most optical components can be monolithically integrated on a chip, which provides a possible route to overcome the above problems. These devices possess the merits of light weight, small size, possible low cost, and on-chip actuation. Therefore, the motivation of this thesis is to develop micro optical sub-systems for enhancing the optical performance of micro optical pickups using the surface micromachining.

1.1 Introduction of miniature pickup heads

In an optical storage system, there are three key components. The disc is for recording data. The spindle is used to rotate the disc when the optical pickup is to read or write the disc. As shown in Fig. 1-1, a conventional optical pickup consists of several individual components, including: (a) a laser diode to supply light source, (b) a

collimator and a prism pair to control the intensity distribution, (c) a polarization beam splitter for beam splitting and a quarter wave plate to control the light direction, (d) an objective lens to focus light to read/write the disc, and (e) a photo diode to receive the signal from the disc.

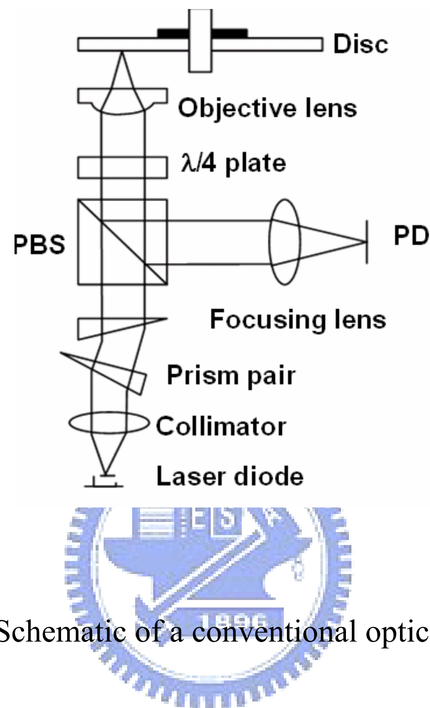

Fig.1-1 Schematic of a conventional optical pickup.

At least four types of micro-optical pickups have been proposed to realize the miniature pickup system: the device of waveguide with a focusing grating[1], the diffractive planar optical module[2], the stacked optical module[3], and the free-space optical bench by surface micro-machining[4]. The waveguide-based pickup was first demonstrated by S. Ura *et al*.[1], as shown in Fig. 1-2. The waveguide was formed with a glass guiding layer and a $Si0_2$ buffer layer on a Si substrate. The miniature pickup was composed of a focusing grating coupler (FGC) and a twin grating focusing beam splitter (TGFBS). The FGC was as a guiding layer of the source laser to make a focused beam for writing/reading the data bit. The TGFBS was as a collector to deflect the reflected wave into four photodiodes near the input laser diode.

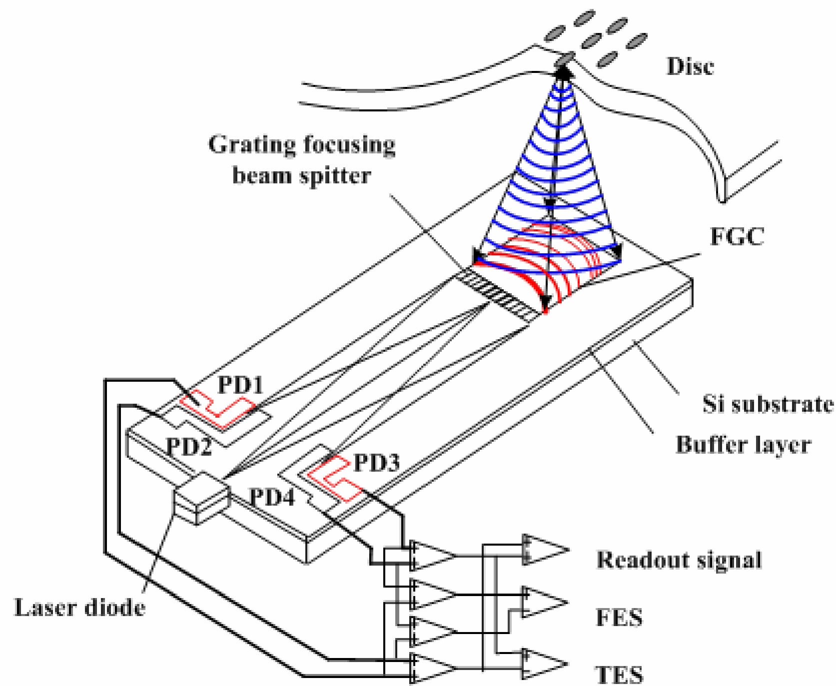

Fig.1-2 Schematic of the integrated optic disk pickup[1].

To apply in high density data storage systems, the spot size, which is correlated with the grating-spacing controlled numerical aperture (NA), has to be reduced. The focus/tracking error signals were processed using the Foucault/push-pull methods. In the absence of the focus error, the pickup was designed so that the reflected beam deflected by the TGFBS focused into the center gap of the neighboring photodiodes. When the disk went away from the pickup, the focus point of the back-coupled guided wave moved away from the FGC, and this beam was absorbed by the outer photodiodes PD(1) and PD(4).When the disk came near the pickup, the focus point of the back-coupled guided wave moved toward the FGC, and this beam was absorbed by the inner photodiodes PD(2) and PD(3). Accordingly, the error signals were employed by the actuators to focus and track. In spite of robustness, this method suffered from high

coupling and propagation loss.

Planar optics based pickup proposed by T. Shiono *et a.l* allowed a double-side diffractive structure to modulate optical propagation. A few minimeters thick glass substrate was used as a light guide, in which the beam followed a zigzag optical path, as illustrated in Fig. 1-3. First, a laser beam was coupled into the substrate containing the optical elements. To stabilize the resonator and avoid wavelength variations, a portion of the light was coupled back into the laser diode by using a reflective feedback lens. The off-axis collimator lens acted to collimate along the oblique optic axis. The twin focusing beam splitter was used to split the forward propagation light from the backward light. Finally, a transmittive off-axis diffractive lens focused the beam onto the disc. On the backward path, the beam was first collimated and coupled into the substrate to hit the twin focusing beam splitter. Another diffraction order of the twin focusing beam splitter was implemented to deflect the light and focus it onto the photodiode segments for tracking and focusing error detections. It was demonstrated that this diffractive planar micro-optic system exhibited stable focusing performance and operated as designed for focus error signal detections. Compared with a waveguide device, the possibility of achieving high performance was higher, because the propagation angle of the optical path could be flexibly designed and the refractive index of the light guide is precisely known. In addition, current lithographic techniques can be used for fabrication as well as submicron alignment precision of the optical elements. Subsequent optomechanical alignment of discrete components or component arrays is not necessary.

However, the off-axis aberrations such as coma and astigmatism significantly deteriorate the overall performance. In addition, alignment error between both sides of the substrate can easily lead to a large amount of stray rays, which potentially cause enormous crosstalk during the reading process.

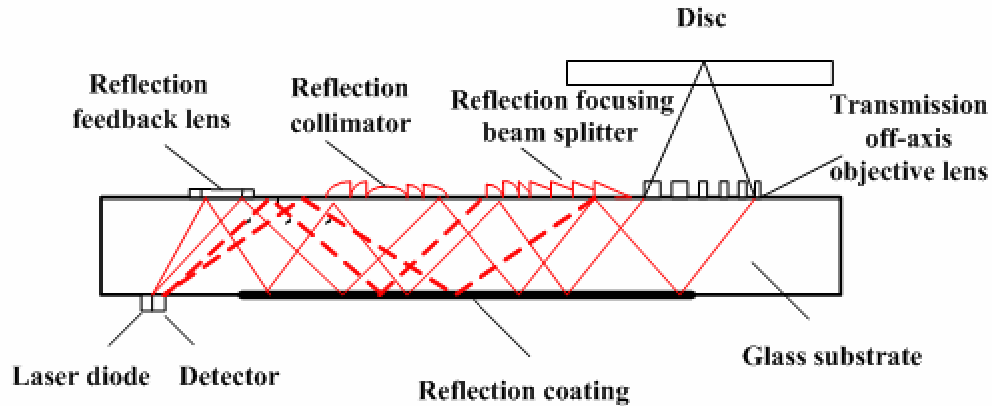

Fig. 1-3. Side view of the planar optical disk pickup[2].

The silicon-based free-space stacked micro-optical pickup was proposed by Chang *et al.* in 2005[8]. The optical pickup system was optically transmissive in both visible and infrared ranges. This device was composed of several optical elements fabricated on the SiN membrane, which was suspended on a Si chip, as shown in Fig. 1-4. It was a three-beam optical pickup system, including an edge-emitting laser die with a 650-nm wavelength, a 45° bulk-mico-machined silicon reflector, a grating to produce three beams, a HOE-based beam splitter, a collimator, a quarter-wave plate and a Fresnel lens as an objective lens. These elements were stacked using chip bonding, thereby significantly reducing the cost, size and weight. The design simplified the process flow. All these qualities made the system more integratable with higher optical efficiency, and fewer off-axis aberrations. The measured spot size was comparable with that of the diffraction-limit. The performance of this device was limited by the alignment error between each layer, the thickness variation of each layer and the quality of the 45° bulk-micomachined silicon reflector.

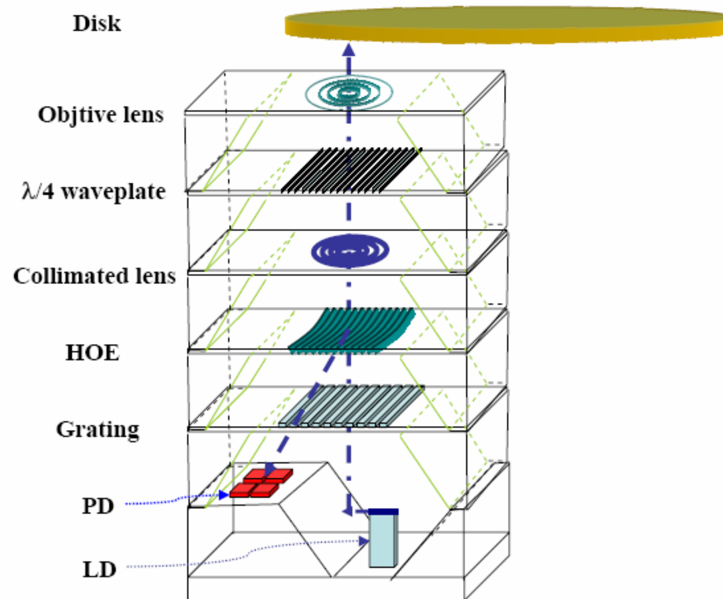

Fig. 1.4. Schematic of the silicon-based stacked optical pickup[3].

In the approach of silicon surface micromachining proposed by M. C. Wu *et al.*, a Si substrate served as a micro-optical bench on which three dimensional optical elements were monolithically fabricated using the micro-hinge technology[4]. The schematic drawing of the pickup is shown in Fig. 1-5. Because the system employed the silicon-based MEMS technology, it was easy to integrate with passive optical elements such as micro fresnel lenses, the grating and the 45° reflectors. These elements can be further integrated with various types of micro-positioners and micro-actuators for precise optical alignment or optical-mechanical switching, such as the rotatable beam splitter. The photo-detector, an active optoelectronic device, can also be added on the Si-substrate, while a semiconductor laser can be attached by assembly. Additional electronic control and signal-processing circuits can be built for controlling the status of micropositioners and the power of the lased diode.

Nevertheless, the approach, employing thin polysilicon film as optical components, suffered from low efficiency because polysilicon film was not transparent to the visible spectrum and the manual assembly procedure was complicated.

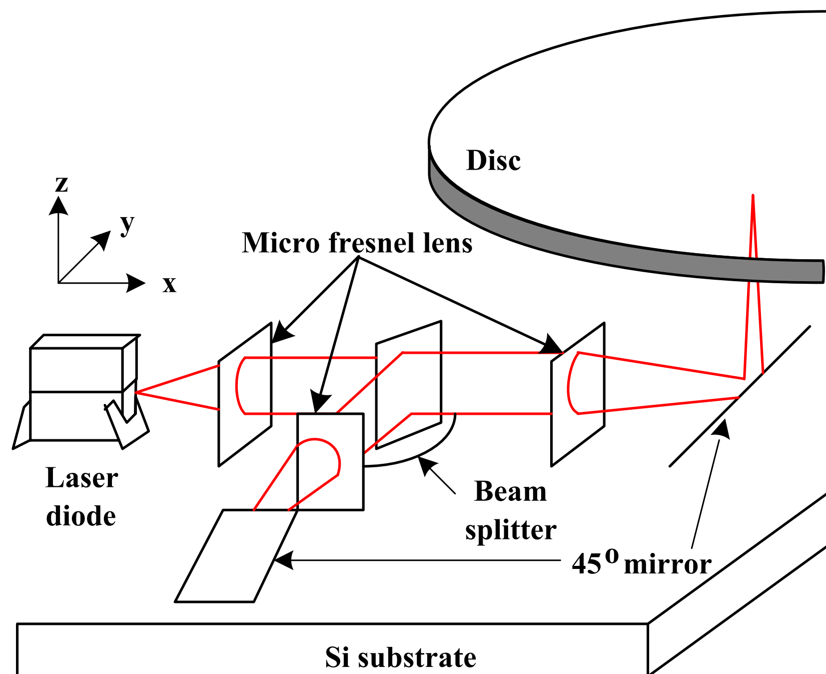

Fig. 1-5 Schematic of a free-space micro-optical pickup on a chip[4].

1.2 Introduction of surface micromachining

To make a micro pickup, one of the methods is using surface micromachining, which adds and patterns materials layer by layer. The common materials in silicon based surface micromachining includes: (a) the structural material, such as the poly silicon or the single crystal silicon; (b) the sacrificial material, such as the phosphosilicate glass (PSG) or silicon dioxide; and (c) the insulator or optical material, such as silicon nitride. The process to make a micro grating is like this. First, an isolator, SiN and a sacrificial layer SiO2 are deposited. After that, the lithography and an etching tool are used to define the dimples. With the similar steps, the first structural layer, poly-si, the optical layer SiN, the second sacrificial layer SiO2, and the second structural layer, poly-Si are defined in sequence. After removing away the sacrificial layer using HF vapor, the device is assembled under the microscope to form a three dimensional structure. As

compared with other micromachining technologies, silicon based surface micromachining is more flexible in both design and fabrication. As shown in Fig. 1-6, a metal layer can be added to make micro actuators and mirrors. Several silicon nitride optical layers can be deposited to make multilayered diffractive elements. Added with bulk micromachining, the optical or electrical connections can be formed. By combining the bonding technology, micro systems can be realized.

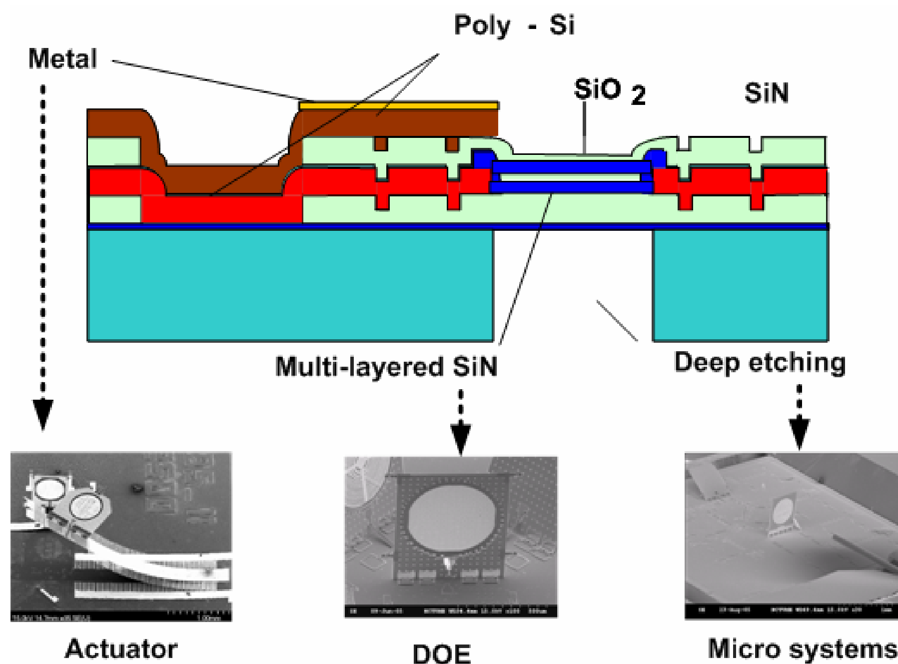

Fig. 1-6. Varities of silicon based surface micromaching.

1.3 Motivation and objective of this Thesis

A comparison of the above four approaches for an integrated-optic pickup device is presented in Table 1-1. Each approach has its pros and cons. Among the proposed miniature pickups, the free-space type is preferred in our research because it possesses more possibility to expand its function such as:

(a) **Replacing the polysilicon film with a low stress silicon nitride film in the optical layer to enhance the optical transmittance in visible light.** The previous

proposed free-space pickup, employing thin-polysilicon film as optical patterns, suffers from polysilicon not transparent to visible light, meaning that it is only compatible with 780 nm CD discs, but not 650 nm DVD discs and 405 HD-DVD discs. Therefore, a low stress silicon nitride film was developed in our research and has been demonstrated to be transparent to visible light.

(b) **Integrating a switchable grating to produce multiple beams in parallel to read a disc at high data rate.** The previous proposed free-space pickup employed a single laser for sequential data retrieving. The data-transfer rate was limited to a beam in reading the disc. To enhance the data retrieving rate, we developed a single/multi-beams switchable grating for 633 nm based DVD system. In a reading state, the switchable grating enhanced the data retrieving rate by producing multiple beams of equal low intensity to simultaneously read several tracks of a disc. In a writing state, the switchable grating produced a beam of high intensity to write a disc.

(c) **Improving the polarization extinction ratio of the micro beam splitter to enhance optical utilization efficiency.** The previous proposed free-space pickup employed a single-layered film as an intensity beam splitter. Limited to its material and simple structure, this beam splitter is not suitable for polarized beam splitting of the visible light. The optical utilization efficiency of the forward/backward light is low. Therefore, we developed a polarized beam splitter (PBS) of high polarization extinction ratio using the thin film optics. It consisted of a novel stack of two low stress and low absorptive silicon nitride layers separated by an air gap. In a free-space pickup, the PBS can integrate with a quarter-wave plate to improve the transmittance of the forward polarized light and the reflectance of the backward polarized light. Moreover, the fabrication of the switch grating and the PBS is compatible with other micro-optical elements, which can be integrated

together to build a multi-function micro optical pickup or other micro-optical systems in the future.

(d) **Developing a micro-reflective system to demonstrate a high rotation angle for fulfilling a CD/DVD/HD-DVD compatible micro-optical pickup.** In the development of optical pickups, the current trend is towards being CD/DVD/ HD-DVD compatible. To realize this function in the micro-optical pickup, one of the solutions is to use a rotary actuator to switch between each light sources, the laser diodes. However, the maximum rotation angle of the surface micromachined rotary actuator is below 2.5 degrees. According to the calculation, it will enlarge the chip size. A proposed micro-reflective system, which possesses the same function of the rotary actuator, is consisted of a prism and a reflector. The design concept is the rotary motion is equivalent the angular to linear conversion and the linear motion. This design can be used to fulfill a CD/DVD/HD-DVD compatible micro-optical pickup.

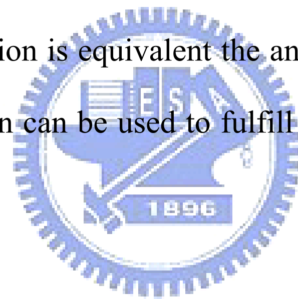
1896

1.4 Organization of this thesis

The thesis is organized as following: In chapter 2, the working principle of a switchable grating and the theories of micro elements, including the micro-hinges, the binary phase grating and the stress-induced actuator, are presented. The topic of chapter 3 includes a summary of micro-fabrication technologies and the instruments to characterize the performance of the switchable grating. Chapter 4 is devoted to"thin film optics", which was used to predict the performance of a micro-PBS with stacked films. The development of low stress silicon nitride films are also described here. In chapter 5, we focus on the structure design and the measurement of the micro-PBS. In chapter 6, we propose and demonstrate the micro-reflective system. In chapter 7, the

main contributions of this dissertation and a proposal of future work are given.

Table 1-1 Pros and cons of the four micro optic pickup heads.

Pros	Cons
Waveguide with focused grating[1]	
1. High integrity	1. Low coupling efficiency 2. Difficult realization of high numerical aperture lens by the grating coupler
Diffractive optical element (DOE) planar approach[2]	
1. Low coupling loss 2. Simple fabrication approach	1. Requirement of precise alignment on both sides of the substrate 2. Low integrity with dynamic devices 3. High off-axis aberration
Stacked optical pickup scheme[3]	
1. Simple design 2. Simple fabrication process	1. Lower integrity with dynamic devices, such as with micro actuators.
Free-space optical bench using the surface-micromachining[4]	
1. High possibility of dynamic calibration in assembly. 2. High possibility to generate a diffraction-limited focused spot.	1. Cumbersome fabrication and assembly process 2. Application only in the infrared spectrum.

Chapter 2

Principles of Microoptics and Microactuators

In conventional CD and DVD drives, an optical pickup (OPU) with a single laser beam is used for sequential data retrieving. The data rate is proportional to the rotation speed of the spindle motor. However, the maximum rotation speed is partly limited by the dynamic characteristics of the objective lens actuator. Using multiple beams in parallel is a straightforward solution to improve the data rate. Several methods have been demonstrated to achieve simultaneous reading of multiple tracks, such as generating multiple beams by using a diffractive optical element[5-6], a diode laser array[7], or a combination of laser diodes and a beam combiner[8]. Alon et al. proposed a pickup using diffractive optical elements[5]. A grating was used to split an illumination beam into multiple beams to read several tracks of the optical storage medium. The reading beams can be generated uniformly by a grating; however, they are not suitable for multi-beam recording due to the insufficient power of each beam. To overcome the limitation, Shih proposed an optical pickup employing a liquid crystal grating to switch alternatively between single-beam recording and multi-beam reading[9]. The liquid crystal grating, however, is of large size and high cost.

In this section, we present the working principle of a micro-silicon-based free-space switchable grating to switch between single-beam recording and multi-beam reading in the micro optical pickup. The switchable grating is composed of a binary phase micro-grating mounted on a bimorph actuator by micro-hinges. Low stress silicon nitride is used as the optical material of the binary phase grating for its high transparency in the visible spectrum and its superior chemical and mechanical

properties. The switching function is achieved using an electrostatic driven stress-induced curved polysilicon based micro actuator.

2.1 Overview of the switchable grating for a micro optical pickup

The free-space integrated micro-optical pickup is based on the surface micromachining technology. As shown in Fig. 2-1, the optical bench, including a collimator, a switchable grating, a polarization beam splitter, a folded mirror and an elliptical diffractive lens are monolithically integrated on a silicon substrate. The vertical binary phase grating is fabricated on a stress-induced actuator and can be raised above the path of the incident beam for data recording (Fig. 1(a)) and lowered to create multiple beams for data retrieving under variable electro-static force. (Fig. 1(b)).

The optical axis of the system is designed to be 400 μm above the silicon substrate. The laser can be mounted on its side with the aid of three-dimensional alignment structures[10] or attached on a 400-μm-thick micro-chip so that its emitting spot is aligned with the optical axis. First, the laser light emitted from the laser diode (LD) is collimated by a micro-fresnel lens or a micro-refractive lens. When the grating is on the optic axis, the forward light is further divided into three beams. Part of the beams passes through the beam splitter. The beam splitter is positioned 45° from the optic axis. The light reflected from the splitter can be used for monitoring the intensity of the LD. The transmitted light is further bent upward by an integrated 45° mirror, which enables the optical bench to be mounted in parallel to the optical disc. After being focused on the disc by the objective lens, the reflected beams carrying the information of the disc are converged by the same objective lens, reflected by the intensity beam splitter, and focused again by an elliptical diffractive lens onto a planar quadrant photodetector attached on the Si substrate.

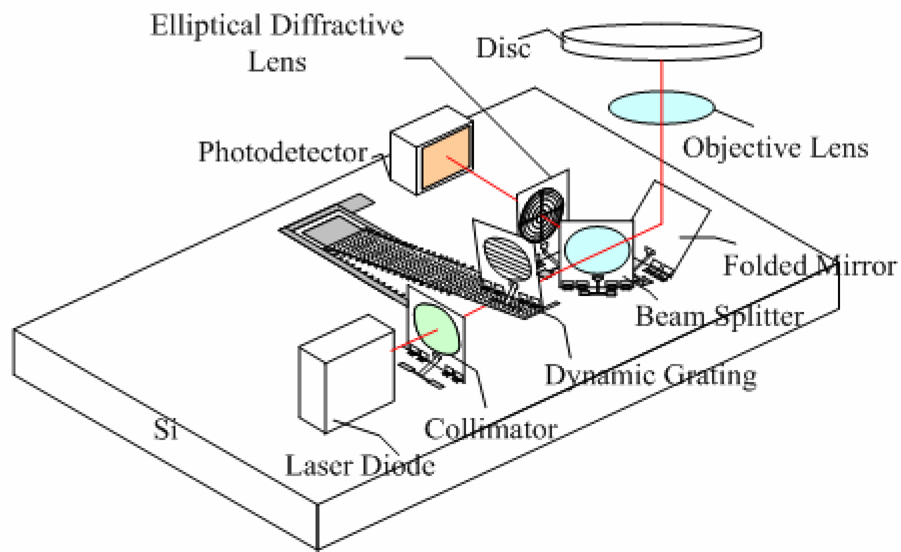

(a) Single-beam state

E S A

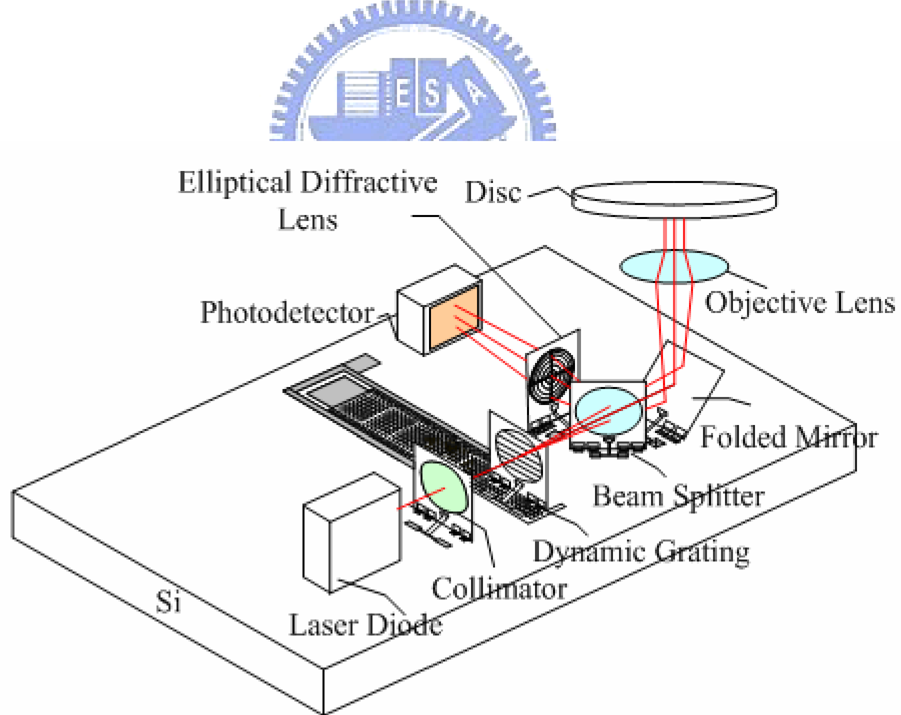

(b) Multi-beam state

Fig. 2-1. Schematic of the micro-optical pickup with a switchable grating: (a) single-beam recording and (b) multi-beam reading.

2.2 Microhinges

In the micro-optical bench, all optical elements are three dimensional and fabricated by the micro-hinge technology with the two layer polysilicon process. Hinged structure was first proposed by Pister in 1991[11]. The structure allows the surface micromachined polysilicon plates to be patterned by photolithography and then folded into three-dimensional structure. There are four types of hinges, as illustrated in Fig. 2-2.

The simplest setup is the 'substrate hinge', as shown in Fig 2-2(a), which consists of a polysilicon (poly-1) plate and a hinge pin constrained by another polysilicon (poly-2) stable. The stable is connected to the substrate through two contact areas, and the plate is free to rotate any degree off the substrate by applying a stop. The width of the pin has to be smaller than the sum of the thickness of the first polysilicon (poly-1) and its sacrifical oxide layers, by which the pin will be able to rotate a full 90 degrees without contacting the substrate and staple. The substrate hinge is used to hinge poly-1 plates to the substrate. In our micro-optical pickup bench, the substrate hinges are applied in the building of the three-dimensional structures of the collimator, the intensity beam splitter, the folded mirror, and the elliptical diffractive lens.

To hinge plates to each other requires the other two types of hinges. Two poly-1 plates can be hinged together using an 'interdigitated hinge', as shown in Fig 2-2(b). Poly-2 strips are connected between interdigitated poly-1 fingers, allowing the plates a relatively 'concave-down' rotation of 180 degrees and preventing the two poly-1 plates from pulling apart.

The third type of hinge is a 'T-style hinge', which hinges two poly-2 plates together and folds 'concave up', illustrated in Fig. 2-2(c). The fourth type of hinge is a 'scissor hinge'[12], which hinges two poly-1 plates together and folds 'concave up', illustrated in Fig 2-2(d). Scissor hinges are the most complicated and also applied in our

micro-optical pickup bench. It is applied to connect the binary phase grating and the stress-induced actuator. The grating is realized using microhinges and spring-latches similar to the substrate-hinge based collimator. However, the hinges of the grating are fixed on the stress-induced actuator instead of Si substrate.

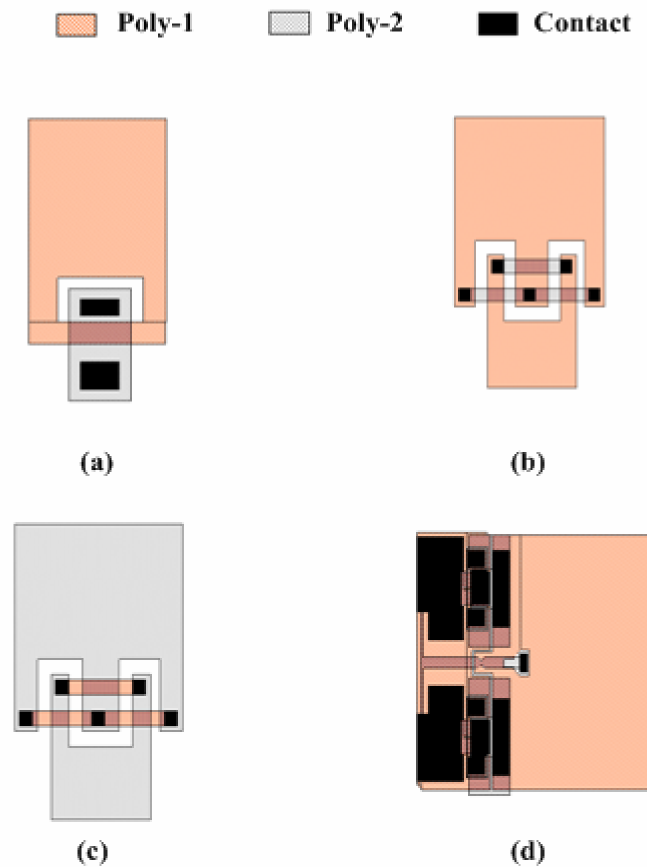

Fig. 2-2. Four types of hinges. (a) Substrate hinge, which is used to hinge released structures to substrate. (b) Interdigitated hinge, which is used to hinges two ‘concave down’ structures. (c) T-style hinge, which is used to hinges two ‘concave up’ structures. (d) Scissor hinge, which is used to hinge two poly-1 plates together and folds ‘concave up’.

Unlike the substrate hinges, there is no ‘pin’ in the other three types of hinges. Given the typical film thicknesses, a substrate hinge designed to rotate 90 degrees must have a pin no more than the total thicknesses of the poly-1, the first and second sacrifical oxide layers. As a result, the other three types of hinges can be applied in all

geometries wider than the above total thicknesses, making them much stronger than substrate hinges.

2.3 Binary phase micrograting

Typical macro-optical components, such as mirror, lens and prism are described by ray optics: treating light as geometrical rays which will be refracted and reflected at optical interface according to the Snell's law. Rather than being refracted at continuous surface profiles, in diffractive optical elements (DOEs) light is diffracted at the periodic microstructure of the element. Specific continuous surface profiles are not easy to be realized in a system sized of a few microns. Therefore, DOEs are more attracted for integrating within micro optical systems. DOEs have several advantages: 1) their diameters as a few hundreds of micrometers can be defined using photolithography; 2) their thickness is on the order of an optical wavelength and suitable for micromachining process[13-15]. To determine the optical path and efficiency of light transmitting in DOEs, scalar diffraction theory and vector diffraction theory are two main theories used to design. Vector diffraction theory is a rigorous electromagnetic theory based on Maxwell equation. Its numerical computing is time-consuming. In contrast, scalar diffraction based on fourier optics is relatively efficient in calculation. If the variation of the surface-relief is larger than the wavelength of light λ, the optical performance except the phenomenon of polarization of DOEs can be dealt with using the scalar diffraction theory[16-18]. Therefore, the scalar diffraction theory is used on the designs in this thesis work.

Binary phase gratings have the stepped approximation with respect to an ideal continuous profile. Diffraction efficiency of binary phase gratings depends on the number of steps in this staircase-like binary profile. In a typical micromachining

process, a sequence of binary processing steps can be used to generate multilevel profiles. Since each step has a specific height, a smart approach is to make 2^N discrete levels by processing N mask lithography and etching. For example, a blazed grating is to deflect the incident light through a certain angle with high efficiency. Fig. 2-3 shows an ideal phase grating profile with a perfect sawtooth profile, and a quantized version of that grating with 2^N level. In this blazed phase grating, if there are 2^N steps of equal spaces and thickness existed in one period Λ with height d, the width and height of each step is $\Lambda/2^N$ and $d/2^N$, respectively.

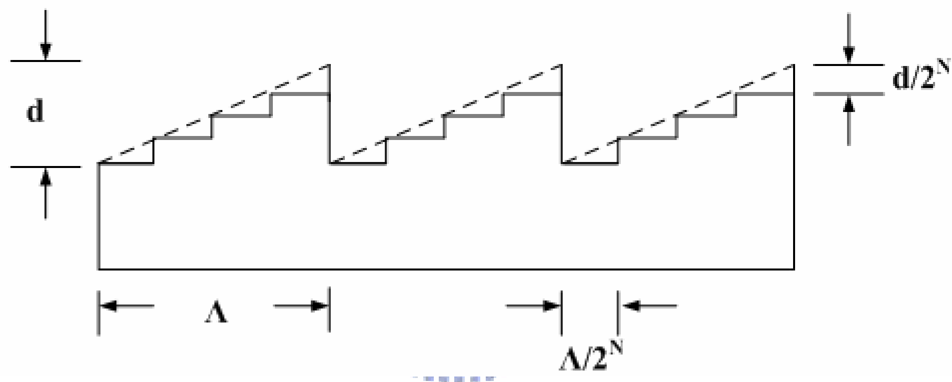

Fig. 2-3. Phase profile comparison between an ideal sawtooh phase profile for a blazed grating, and a binary approximation to that profile.

However, the precision of the lithography process is limited. As described above, the fabrication process for multilevel phase elements generally consists of a sequence of binary fabrication steps each of which requires an aligment and an etching step[19-21]. Alignment errors occur if the masks for subsequent lithographic structuring processes are slightly shifted relative to existing structures. Etching errors occur if the phase step introduced during individual etching processes deviates from the ideal step profile with precisely defined etching depth and vertical edges. Since our target is to demonstrate the possibility of a switchable grating, a two-level phase grating with rectangular shape

was selected to reduce the process complexity. Under the specific conditions, this two-level phase grating can produce three beams of equal intensity.

To apply the three beam grating in an optical pickup, the diffraction ratio, η, of the 0th order beam intensity I_0 and the $\pm1^{st}$ order beam intensities $I_{\pm1}$ should be controlled to approach one. In addition, the power efficiency, $\eta_u=(I_{-1}+I_0+I_{+1})/I_{input}$, where I_{input} is the intensity of the input beam, should be as high as possible. The diffraction angle between the 0th order and the $\pm1^{st}$ order beams is determined by the optical system layout such as the working distance, the thickness of the cover layer of the disc, and the spacing between the 0th and the $\pm1^{st}$ order beams on the disc, as shown in Fig. 2-4.

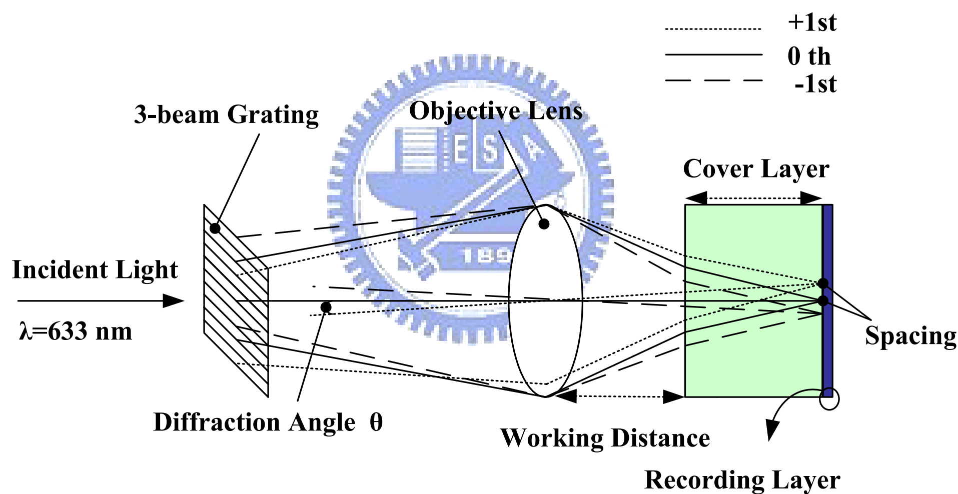

Fig. 2-4. Optical path of the three beams for reading.

To determine the diffraction angle of the first-order beams, we assumed 40-μm spacing between individual focused spots on the disc. Because the spot spacing is larger than the track pitch, the array of spot would be positioned at an angle from radial direction in practical applications. The micro-pickup is designed to read a disc, which has a 100-μm thick cover layer with refractive index n= 1.6. If the working distance

between the objective lens and the cover layer is 460 μm, under the thin lens approximation for the objective lens, the diffraction angle, θ, is about 4.35°. For a transmissive grating with θ=4.35°, m=1 and λ=633 nm, the period Λ is about 8.35 μm, derived from the equation Λ×sinθ=m×λ. Λ=8 μm was selected in the design. To reduce the process complexity, a grating with rectangular shape was used.

The power in the diffracted beams I_0 and $I_1$of the grating can be determined by the period Λ, the line-width w and the depth of the grating D as follows[22];

$$I_O = (2f-1)\sin\phi^2 + \cos^2\phi \tag{2-1}$$

$$I_1 = [2(\frac{\sin m\pi f}{m\pi})\sin\phi]^2$$

where m=1 is the diffracted order, fill factor f=w/Λ is the ratio of the line-width to the grating period and phase shift ϕ is related to the depth of the grating D and the refractive index *n* of the grating material by the formula

$$\frac{D(n-1)}{\lambda} = \frac{\phi}{180} \tag{2-2}$$

where n=2.102+0.008i is the measured index of refraction of low-stress silicon nitride at λ=633 nm. According to pre-run simulations, it was found when the fill factor was 0.50; multiple grating depths could be used. For example, 101 nm (η_u =81.7%), 404nm (η_u =83%), and 657nm (η_u = 74.7%) satisfied the desired diffraction efficiency ratio. Other grating depths meeting the requirement were higher than 1000 nm, which was not suitable in surface micromachining processes. To have sufficient mechanical strength and reasonable fabrication yield, the depth of 404 nm was selected, which also yielded high energy utilization efficiency. The contour plot of the diffraction ratio $I_0/I_{\pm1}$ is shown in Fig. 2-5 as a function of the fill factor f and the grating depth D. As can be seen, a diffraction ratio $I_0/I_{\pm1}$ of about 1 can be obtained provided that f=0.5 and

D=404nm.

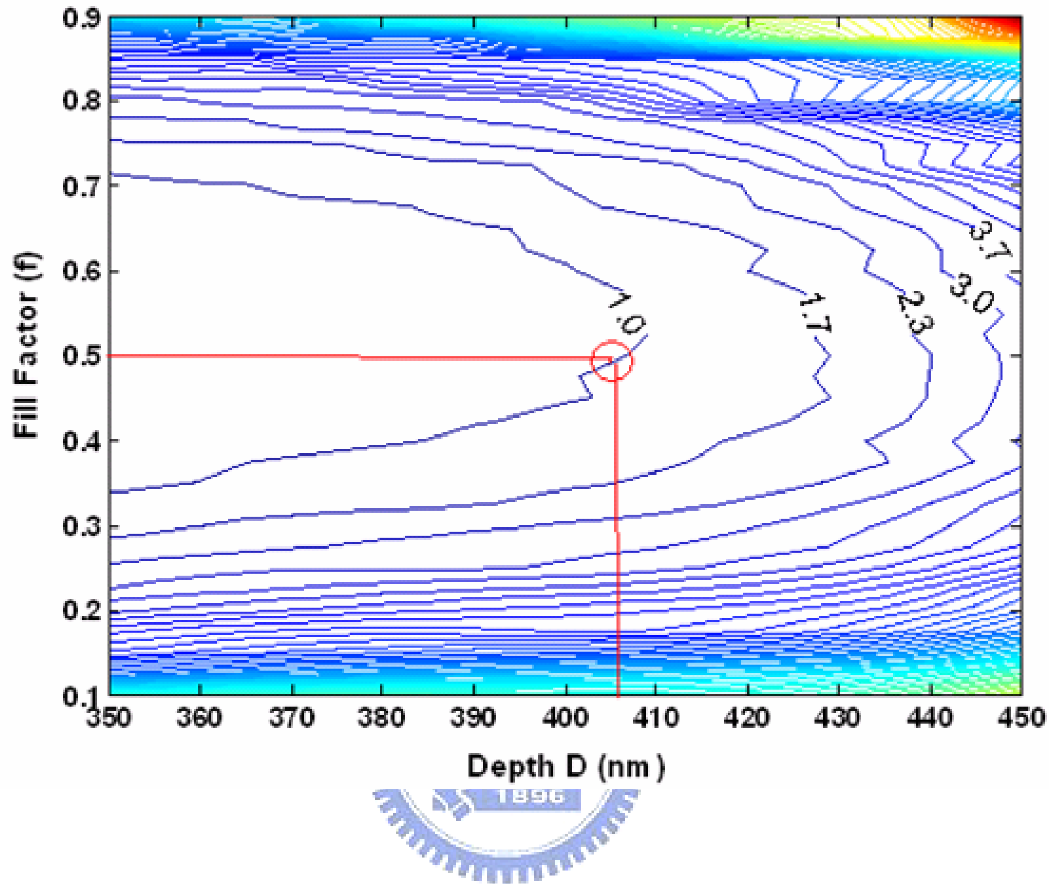

Fig. 2-5. Diffraction ratio ($I_0/I_{\pm1}$) contours.

According to pre-run simulations, it was found when the fill factor was 0.50; multiple grating depths could be used. For example, 101 nm (η_u =81.7%), 404nm (η_u =83%), and 657nm (η_u = 74.7%) satisfied the desired diffraction efficiency ratio. Other grating depths meeting the requirement were higher than 1000 nm, which was not suitable in surface micromachining processes. To have sufficient mechanical strength and reasonable fabrication yield, the depth of 404 nm was selected, which also yielded high energy utilization efficiency. The contour plot of the diffraction ratio $I_0/I_{\pm1}$ is shown in Fig. 2-5 as a function of the fill factor f and the grating depth D. As can be

seen, a diffraction ratio $I_0/I_{\pm1}$ of about 1 can be obtained provided that f=0.5 and D=404nm.

2.4 Stress-induced micro-actuator

Many new surface-micromachined microactuators have been proposed and demonstrated to integrate various optical elements since the invention of micromotors. Some schematic of these microactuators are illustrated in Fig. 2-6. The comb drive is actuated by applying electrostatic force between the movable combs and the fixed combs, as shown in Fig. 2-6(a). Micronewtons of force and a few micro-meters of displacement are produced by typical surface-micromachined polysilicon comb drive actuators, which have been demonstrated to drive optical choppers[23] and bar-code scanners[24]. The linear microvibromotor is actuated by the impacts from the comb drives. The linear microvibromotor shown in Fig. 2-6(b) consists of a set of resonant comb drives and a slider. By adjusting the number and the frequency of impacts, a sub-micron positioning resolution and a travel range exceeding 100μm has been achieved[25]. The linear microvibromotor has been employed to actuate a slider dragged mirror to align optical beams for fiber coupling[26]. On the other hand, the thermal actuator is actuated by thermal expansion difference between a “cold” arm and a “hot” arm in a U-shaped geometry as shown in Fig. 2-6(c). By applying a 10 mW driving power, a deflection up to 16 μm and force of 4.4 μN has been achieved by the polysilicon thermal actuators[27], which can be used to assemble three-dimensional structures[28]. The scratch drive actuator (SDA) is actuated by applying pulses of electric bias between the polysilicon plate and a bottom electrode separated by an insulator film (Si_3N_4), as shown in Fig. 2-6(d). By adjusting the amplitude and the frequency of pulses, a sub μm step size, 20-30 nm, has been achieved[29]. The SDA is

ideal for positioning optical elements that require accuracy below 0.1μm[30] and has been applied in the optical switches[31] and the variable optical delay line[32].

To design a switchable grating for a micro-optical pickup, the actuator has to switch alternatively between the state of single beam and the state of multiple beams. The actuation distance in the free end of the bimorph actuator needs to be larger than the illumination range of the incident beam on the optical axis. In a standard electrostatic parallel-plate actuator, actuation distance is determined by the balance between the electrostatic force and the mechanical restoring force. For a linear restoring force, the controllable actuation distance is only one third of the gap between two parallel electrodes[33]. To overcome the limited actuation distance, Rosa *et al*. proposed an external electrode bi-morph actuator to operate over the entire range of motion by preventing electrostatic pull-in instability[34]. However, the electrical fringe effect between the moving and the fixed external electrodes is relatively insufficient to obtain enough actuating force. Accordingly, the bimorph actuator used in our research is based on the design demonstrated by Chiou et al.[35], which used comb-shape external electrodes and post heat treatment to achieve higher actuation distance under lower voltages.

In our design, the stress-induced actuator is a composite cantilever, composed of a polysilicon layer and a gold film. The cantilever bends upward since polysilicon has a small compressive residual stress while the gold film has a large tensile residual stress. Schematic of the polysilicon-gold composite cantilever is shown in Fig. 2-7. The curvature and tip deflection of the cantilever were determined by its geometric dimensions and material properties. The curvature of the beam is expressed by the equation[36].

$$\frac{1}{\rho} = \frac{6(m\sigma_2 - \sigma_1)}{hE_2(3m + K[n(1+n)^2]^{-1}} \tag{2-3}$$

where σ_1 and σ_2 are the residual stress of polysilicon and gold. E_1 and E_2 are the Young's modulus of polysilicon and gold.

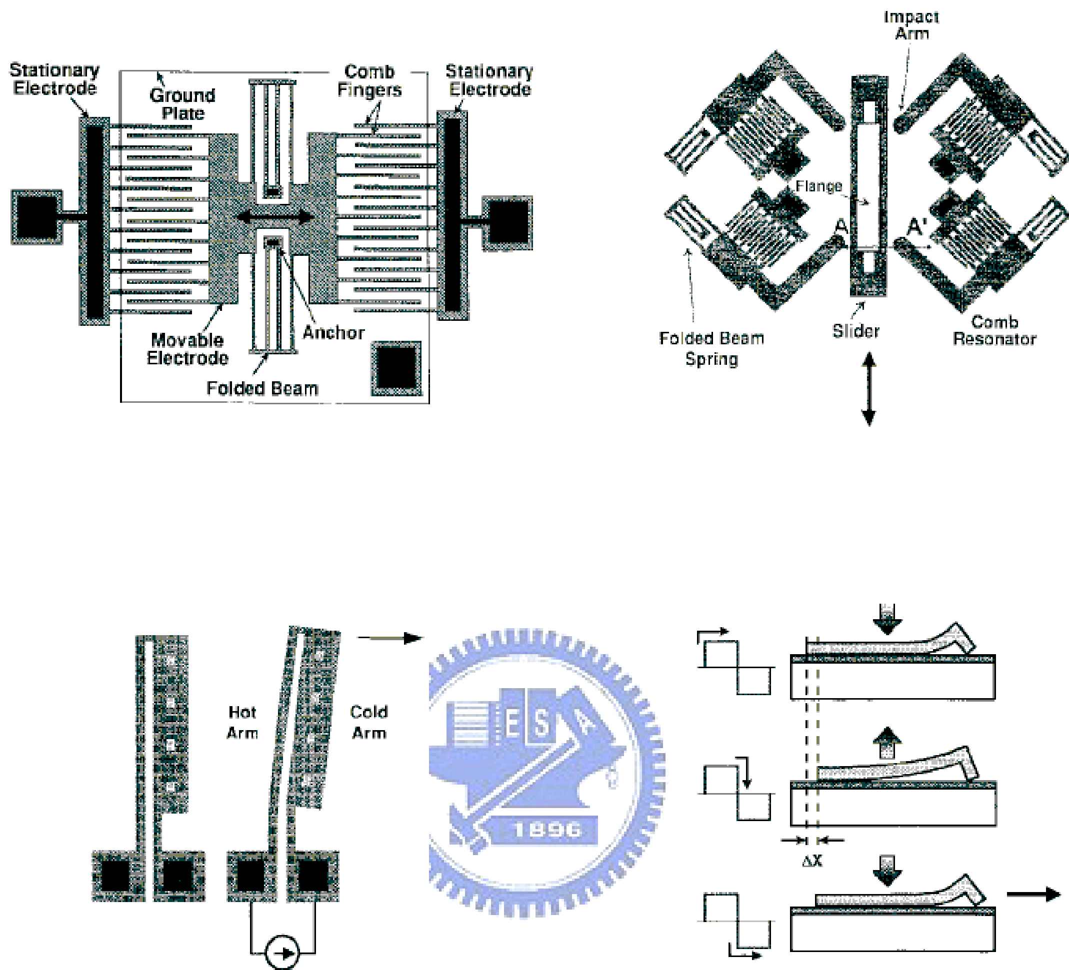

Fig. 2-6. Schematic of microactuators commonly used in surface-micromachined optical systems: (a) comb drive actuator[23], (b) linear microvibromotor[25], (c) thermal actuator[27], and (d) scratch drive actuator[29]. (a)

The symbol m=E_1/E_2, n=h_1/h_2 and K is related by

$$K = 1 + 4mn + 6mn^2 + 4mn^3 + m^2n^2 \tag{2-4}$$

where h_1 and h_2 are the thickness of polysilicon and gold. With the radius of curvature ρ and the length L known, the maximum deflection δ at the tip of the beam, where the grating is positioned, can be expressed as

$$\delta = \rho[1 - \cos(\frac{L}{\rho})] \tag{2-5}$$

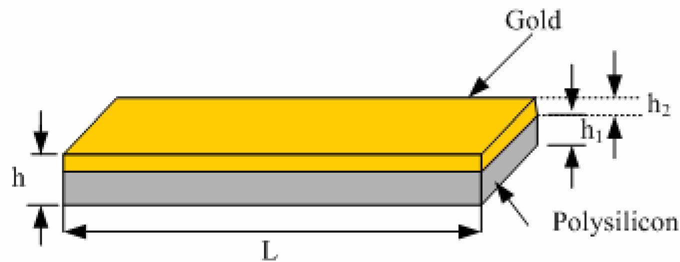

Fig. 2-7. Schematic representation of dimensions of the polysilicon-gold composite cantilever.

According to Equations (2-3)-(2-5), a 140-nm-thick Cr film and a 0.5-μm-thick Au film will be deposited on a 2-μm-thick polysilicon to curve up the composite cantilever. The length of the designed cantilever is 2000 μm. As illustrated in Fig. 2-8, the proposed switchable grating consists of a 2000 × 260 μm^2 bimorph beam anchored to a bonding pad and a binary phase grating attached to the other end using microhinges and microspring latches. Movable comb fingers are connected to the bimorph beams on both sides; fixed comb fingers are connected to the nitride isolation layer on the surface. The engaged length of the comb finger is 180 μm. To actuate the switch, a voltage about 80 volts will be applied between the fixed and movable fingers. The fringing electrostatic field can then pull the curled bimorph beam down toward the substrate.

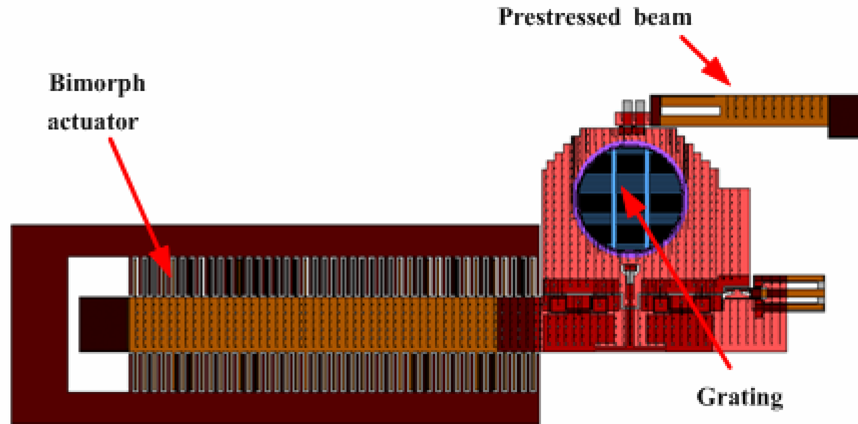

Fig. 2-8. Layout of the proposed switchable grating mounted at the end of a bimorph actuator. The pre-stressed beam is used to assist lifting the released grating during the assembly.

2.5 Summary

The technologies used to design a switchable grating, including microhinges, the binary phase rating and the stress-induced actuator, have been briefly discussed in this chapter.

We presented the fundamental forms and function of four types of microhinges. To meet the demand of the switchable grating, scissor hinges were selected to fix the binary phase grating on the tip of the stress-induced actuator. The mechanism and fabrication issues of binary phase gratings were also discussed. Considering our fabrication tool, three diffracted beams with equal intensity from the grating were designed according to the requirement of the pickup systems. The three beams of equal intensity were achieved by adopting a phase grating composed of silicon nitride (refractive index n=2.102+0.008i) with fill factor f=0.5 and profile depth D=404 nm.

The stress-induced actuator was a composite cantilever, composed of a 2-µm-thick polysilicon compressive layer and a 0.5-µm-thick gold tensile film. To actuate this switch, a voltage about 80 volts will be applied between the fixed and movable fingers.

The fringing electrostatic field can then pull down the curled bimorph beam with the grating toward the substrate.

Chapter 3

Fabrication and Measurement of Switchable Grating

The multi-beam optical pickup was fabricated by a two-layer polysilicon and one-layer silicon nitride surface micromachining process. A process overview of the process is discussed in Section 3.1. The released and antisticion process is presented in Section 3.2. After that, the multi-beam optical pickup fabricated by the above-mentioned process is described in Section 3.3. The final section is the measurement result.

3.1 Manufacturing process

The two-layer polysilicon and one-layer silicon nitride surface micromachining process is derived from the Multi-User MEMS Process (MUMPs), which was developed at the Berkeley Sensors and Actuators Center (BSAC) at the University of California in the late 80's and early 90's[37]. To integrate optical elements in a poly-silicon frame, a low stress silicon nitride film was added. The process begins with 150 mm (100) silicon wafers of 1-2 Ω-cm resistivity. First a 600 nm low-stress LPCVD (low pressure chemical vapor deposition) silicon nitride layer is deposited on the wafers as an electrical isolation layer. This is followed directly by a 2.0 µm silicon dioxide sacrificial layer deposited by PECVD (plasma enhanced chemical vapor deposition) and annealed at 950°C for 0.2 hour in $POCl_3$. This layer of $POCl_3$-doped silicon dioxide, known as the first sacrifical layer, is removed at the end of the process to free the first

mechanical layer of polysilicon.

The sacrificial layer is lithographically patterned with the first mask (DIMPLE) using photoresist AZ4620 and the dimples are then transferred into the first sacrificial layer in an RIE (reactive ion etch) system. The etched depth of the dimples is controlled to be 750~800 nm. The wafers are then patterned with the second mask (ANCHOR1) and reactive ion etched. This step provides anchor holes that will be filled by the first polysilicon layer. After etching ANCHOR1, the first structural layer of polysilicon is deposited with a thickness of 2.0~2.2 μm. The wafer is annealed at 1050°C for 1 hour to significantly reduce the residual stress in the polysilicon layer.

The polysilicon is lithographically patterned using the third mask (POLY 1) to define the first structural layer. In this step, a 8 μm AZ4620 photoresist is produced as a mask for the subsequent polysilicon etch. The thick photoresist is more resistant to the etching chemistry than a thin photoresist. After etching the polysilicon, the photoresist is stripped using acetone and standard cleaning process. After Poly 1 is etched, a ~450 nm low stress silicon nitride optical layer is deposited and annealed at 1050°C for 1 hour in nitrogen to lower the tensile stress of the the silicon nitride. The silicon nitride is lithographically patterned using the fourth mask (LSiN) to define the optical pattern. In this step, the linewidth has to be precisely controlled, which can be confirmed by AFM (atomic force microscopy). After the silicon nitride being reactive ion etched, a second 2.0 μm silicon dioxide sacrificial layer is deposited by PECVD and annealed annealed at 950°C for 0.2 hour in $POCl_3$. The second silicon dioxide layer is patterned with the fifth mask (VIA) and reactive ion etched. The VIA level defines etch holes in the second silicon dioxide layer down to the first structural layer to provide a mechanical and electrical connection between the first and the second polysilicon layers. The etched depth of the VIA holes is controlled to be 2.0~2.1 μm.

After etching VIA, the second structural layer of polysilicon is deposited at a

thickness of 1.5 μm. The wafer is annealed at 1050°C for 1 hour to significantly reduce the residual stress in the second polysilicon layer. The second polysilicon layer is lithographically patterned with the sixth mask (POLY2). The polysilicon layers are etched by RIE processes, similar to those used for Poly 1. The photoresist is stripped using acetone and standard cleaning process. The final deposited layer is a 0.5 μm gold layer for inducing curve-up stress, probing, bonding, electrical routing and highly reflective mirror surfaces. The wafer is patterned lithographically with the seventh mask (METAL) and the metal is deposited and patterned using 10 um photoresist lift-off process. The final, unreleased structure is shown in Fig. 3-1. Table 3-1 lists the thickness of each layer in the surface micromachining process. The wafers are diced and sorted for sacrificial release and test.

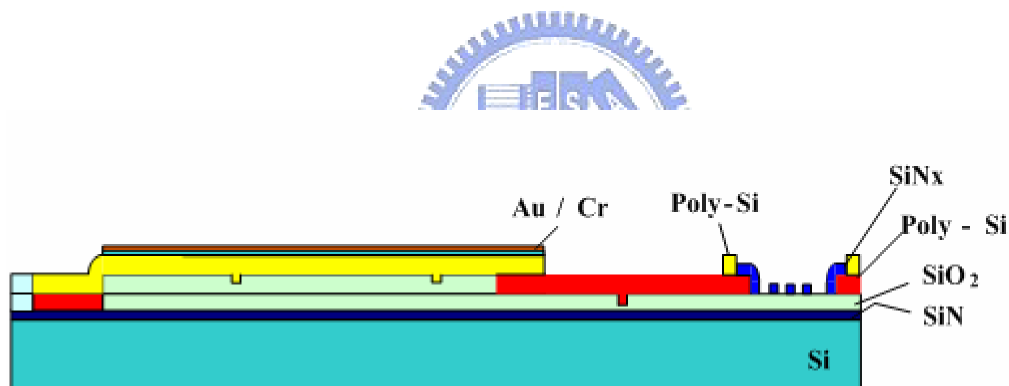

Fig. 3-1. Cross sectional view showing all 7 layers of the surface micromachining process.

Table 3-1: Thickness of each layer in polysilicon/silicon nitride process

Layer	Thickness (μm)
Metal (Au)	0.5
Poly 2	1.5
2nd Oxide	2
LSiN	0.45
Poly 1	2
1st Oxide	2
Nitride	0.6

3.2 Release and anti-stiction process

The release process, a post process of surface micromachining, is employed to remove the sacrifical layers such that the designed structural layers can be freed. After the dicing, HF(hydroflouric) acid or vapor is used to release the micro-structures. The micromechanical structures are vulnerable to stiction, which is induced by interfacial forces due to their large surface area-to-volume ratio and thin air-gap between adjacent surfaces[38-39]. Thus, releasing micro-structures with lower stiction has been an issue in surface micromachining. In most cases, the SiO_2 acrificial layer is removed by HF wet etching and followed by deionized water rinsing and drying. The release-related stiction occurs at the drying step due to possible causes: Van Der Waals force, electrostatic force and contamination[40-41]. Conventionally, to significantly alleviate the stiction problem, super critical drying process is utilized[42]. It is a time-consuming procedure. Our release procedure is derived from HF vapor-phase etching, which is not a real dry process, because water molecules are always produced on the etching surfaces, and a portion of them is condensed to form liquid-phase[43-45]. Since the water condensation can be minimized by high substrate temperature, a 40-watt lamp is used during our releasing procedure. The home made release instrument is shown in Fig. 3-2. The

release procedure is as follows:

(1) Soak chips for 20 minutes in acetone to remove photoresist.

(2) Soak chips for 10 minutes in heated sulfuric acid and 10 minutes in DI water.

(3) Put the chips in a Teflon mesh holder mounted on top of a HF solution container with a transparent plastic cap.

(4) Illuminate the chips for 30 minutes under a 40 watt lamp.

(5) Heat the chips on the hot plate for 20 minutes at 90℃.

After above steps, release process under an anti-stiction condition is accomplished. The molecular byproducts from release can be significantly reduced. The capillary problem is efficiently alleviated.

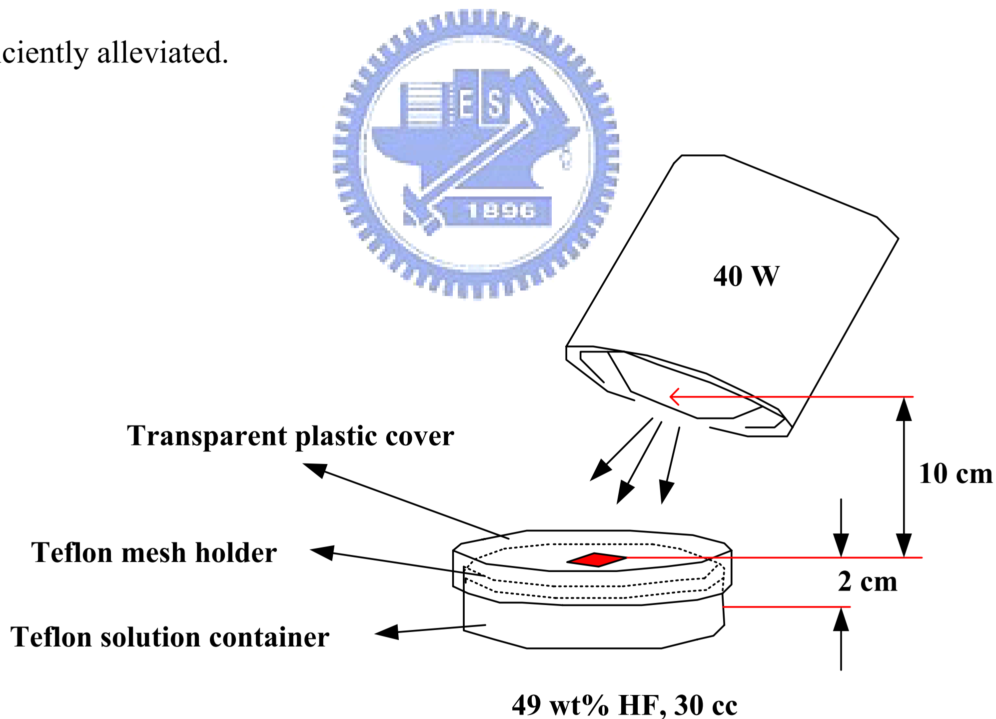

Fig. 3-2. Schematic of the home made release instrument including a 40 watt lamp and a set of Teflone tools.

3.3 Realization of switchable grating

To fabricate the device, an isolation layer of 0.6 μm thick silicon nitride (SiN) was first deposited. After growing a 2-μm-thick sacrificial silicon dioxide (SiO_2), 0.7-μm-deep dimples and 2-μm-deep anchors were then patterned in the sacrificial layer shown in Fig. 3-3(a). The first structural poly-Si and optical layer SiN_x were then deposited and patterned to form a frame shown in Fig. 3-3(b). The thickness of SiN_x layers would be further reduced to the target value at the HF releasing step. After growing a 2-μm-thick SiO_2 and patterning anchors, the second structural poly-Si layer was deposited and patterned to implement the micro-spring latches and the first layer of cantilever beam. The wafer was annealed for two hours at 1050℃ in nitrogen to reduce the residual film stress. A 140-nm-thick Cr film and a 0.5-μm -thick Au film were deposited on the cantilever to induce the internal stresses shown in Fig. 3-3(c). Upon releasing in hydrofluoric (HF) vapor at 40 ^{o}C, the cantilever beam curved upward to lift the micrograting off the substrate. A micro-probe was then used to assemble the micrograting to vertical position, as shown in Fig. 3-3(d). The SEM micrograph of the switchable grating with a central aperture of 500 μm in diameter is shown in Fig. 3-4(a). Using the same process, the switchable grating was integrated with other components to form the micro optical pickup shown in Fig. 3-4(b).

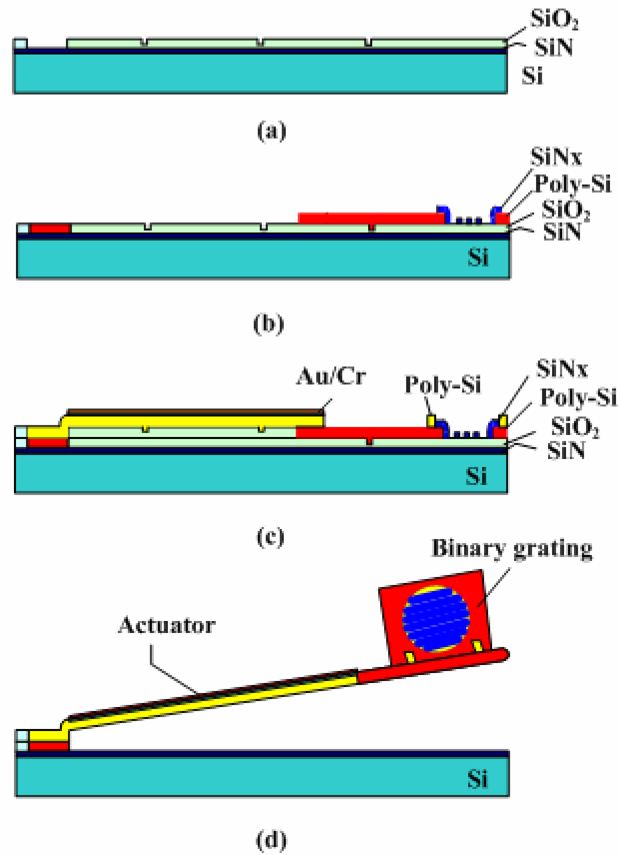

Fig. 3-3. Process flow for the switchable grating: (a) dimple-etch and anchor-etch after the first silicon dioxide deposition. (b) silicon nitride patterning after the first poly-silicon. (c) Cr/Au films and the second poly-silicon patterning after the second silicon dioxide deposition and the second anchor-etch. (d) releasing and assembly.

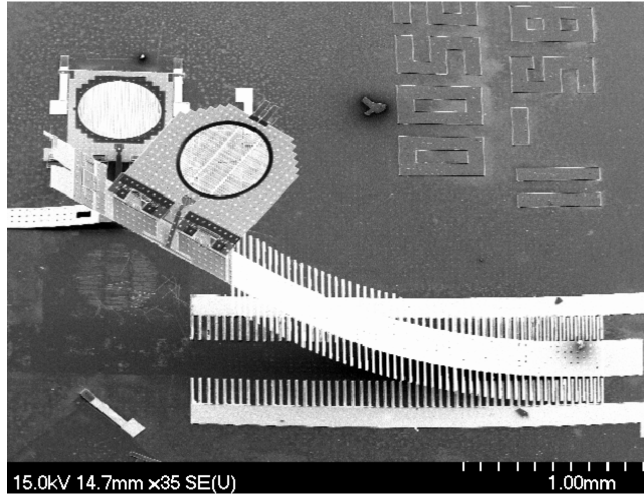

(a)

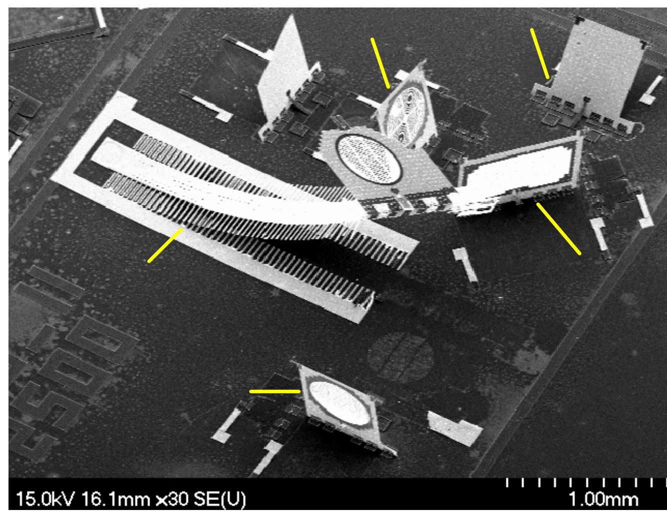

(b)

Fig. 3-4. SEM of a (a) switchable grating and (b) micro optical elements in an optical pickup.

3.4 Experimental results and discussions

The static characteristics of the bimorph actuator with a grating were obtained by applying a dc bias driving voltage at the fixed comb fingers. The measured lift height of the free end versus the applied dc bias driving voltage is shown in Fig. 3-5. Between 24

volts and 64 volts, a steep gradient was observed for the electrostatic force from the comb fingers overwhelming the restoring force of the stress-induced curved beam. After 64 volts, the gradient reduceed for most movable comb fingers contacting the substrate. This figure shows that to lower the grating down to the silicon substrate, the applied voltage has to be larger than 80 voltages.

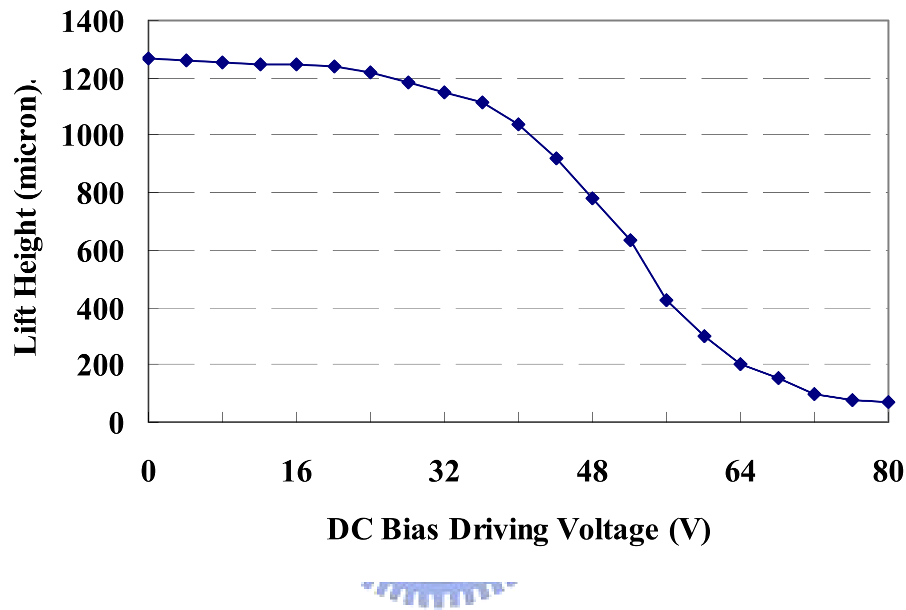

Fig. 3-5. Static lift heights of the free end versus dc bias driving voltages.

To measure the optical performance of the micro devices, a He-Ne laser at λ=632.8nm was used as the light source. To block optical noises from outside of the optical pattern area, an aperture of a diameter 350 μm was used to yield the incident beam size, which was smaller than the grating area of a diameter 500μm. The beam alignment tolerance was 75μm in the measurement. A polarizer was adjusted to obtain the required polarization states. The optical patterns were measured by a CCD camera positioned at 10 mm from the switchable grating.

As shown in Fig. 3-6(a), when no voltage was applied, the incident beam propagated directly for recording use. As shown in Fig. 3-6(b), an external voltage of 80 volts was applied to have the incident beam pass through the binary phase grating for reading use. For the micro-grating, the measured Gaussian beam widths of the -1st, 0th, and +1st order beams were 271 μm, 293 μm, and 278 μm, respectively, which implied the diffraction intensity distribution was symmetric. The measured diffraction angle at far field was 4.51°, which agreed well with the theoretical value of 4.53°. The normalized measured intensities of the -1st order beam, 0th order beam and the +1st order beam are 0.93,1 and 0.91, respectively. There was 57.1% of the incident power distributed among the three useful orders whereas the calculated efficiency was 67.6%. The deviation from the target value of 1 for each beam was mainly due to the thickness variation, index variation, dimples, the roughness of the sidewall and the surface of the grating. The mean roughness was 5.3 nm, which introduced phase variation and affected the energy distribution of the diffracted beams.

The thickness variation and roughness of the silicon nitride film as influenced by film growth and HF releasing can cause phase differences and scattering of the light at the interface. Besides, the thermal stress between the silicon nitride film and the poly-silicon plate distorted the intensity profile of the main beam.

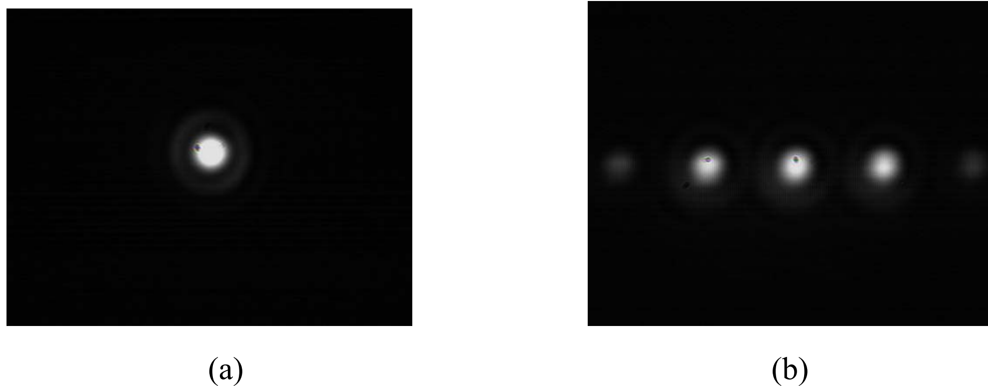

(a) (b)

Fig. 3-6. Diffraction patterns (a) before and (b) after applying voltage to the actuator.

3.5 Comparisons

A comparison of the stress-induced with the liquid crystal based switchable gratings is listed in table 3-2. Among the four characteristic items, the stress-induced switchable grating requires higher driven voltage and produces fewer beams. But its size is smaller by 2 orders. Its process compatibility with other optical components is also better.

For the large driven voltage issue, the structure can be further optimized to reduce its driven voltage. For example, the tip height (1250 μm) is above the requirement (800 μm). By reducing the tip height, the driven voltage is lessened. The thickness of the stress beam can be reduced from 2 μm to 1.5 μm to induce the spring constant and thus the driven voltage. Besides, the coupling length between the movable and fixed comb fingers can be increased to reduce the driven voltage according to [35]:

$$F_E = \frac{1}{2} * N * L_c * \frac{dC}{dZ} * V^2 \tag{3-1}$$

where N is the number of the comb fingers, Lc is the coupling length of comb fingers, dC/dZ is the gradient of capacitance of comb fingers in z direction, and V is the applied driven voltage. According to formula (3-1), the driven voltage can be lowered from 80 volts to 60 volts if the coupling length increases from 180 μm to 300 μm.

For the few diffraction beam issue, a 7-beam grating can be designed to replace the current 3-beam grating, but the width tolerance would be reduced from ±0.4 μm to ±0.1 μm. Another solution is to use a cascaded grating array, as shown in Fig. 3-7.

Table 3-2: Comparison of liquid crystal and stress-induced switchable gratings

	Liquid Crystal	Stress-induced
(1) Drive voltage	2.4 V	80 V
(2) Beam Number	7 beams	3 beams
(3) Volume	~1 cm3	~0.005 cm3
(4) Process	Poor	Good

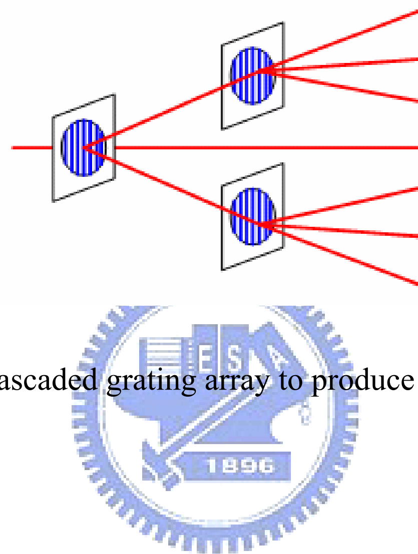

Fig. 3-7. Schematic of a cascaded grating array to produce seven diffraction beams of equal intensity.

1896

3.6 Summary

Using a two-layer poly-silicon and one-layer low stress silicon nitride surface micromachining process, a switchable micro-grating composed of a binary phase grating and a bimorph actuator was demonstrated. The optical pattern area of the grating was 500 μm in diameter. The voltage required to switch the grating was 80 volts. The measured diffraction angle was 4.51°. The normalized measured diffraction intensities of the -1st order beam, 0th order beam and the +1st order beam were 0.93, 1, and 0.91. The optical performance of the dynamic grating shows its potential for integration with other micro-optical elements for multibeam optical pickups application in the future.

Chapter 4

Polarization Beam Splitter

High-extinction-ratio micro polarizing beam splitters (micro PBS) are required in micro optical systems for sensing and signal processing when the polarization state is a concern. For example, in an optical storage system, a high-extinction-ratio micro PBS is required to divide the incident light into a highly reflected TE mode and a highly transmitted TM mode to reduce the optical noise. The reflected TE mode is used to monitor the light intensity; the TM mode is used to read and write the data on the disk. A surface micromachined poly-silicon PBS was first proposed by Pu *et al.* and demonstrated to operate well for near IR[46]. For short wavelength applications, such as 405nm for blue light storage system, the poly-silicon based PBS is not suitable due to its high absorption. Among the materials used in polysilicon based surface micromachining, silicon nitride and silicon dioxide have high transparency in the visible spectrum range[47]. However, silicon dioxide is usually used as the sacrificial layer. Therefore, silicon nitride was investigated as the optical material.

Employing the polarization sensitive characteristic of the dielectric film, a silicon nitride film at the Brewster angle incidence can serve as a PBS. To achieve higher polarization extinction ratio, multilayer coating on the PBS surface or cascading several PBS's in tandem are required. The former method is limited by the materials available in surface micromachining, while the latter requires large area and operates only for the transmitted waves. To overcome the constraints of available materials and die size, a SiN/Air/SiN stack operating at the Brewster angle incidence is first proposed to replace the conventional multilayer coating. The stack is composed of

two silicon nitride layers (as high-refractive-index layers) separated by an air gap (as a low-refractive-index layer). At the Brewster angle incidence, the reflectivity of the TM mode will be nominally zero. By choosing specific thicknesses of the silicon nitride layers and the air gap, the reflectivity of the TE mode can be higher than 90%, leaving the transmitted light almost TM mode.

When combined with poly-silicon structures, a high-extinction-ratio pop-up micro PBS can be fabricated and easily integrated with other micro optical elements, such as a cylindrical lens to shape the incident beam, a grating to form tracking beams, a micro astigmatic lens to slightly alter the horizontal and vertical focal distances of the resulting spot on the photodiode array and mirrors as the reflectors, to form a micro optical pickup for short wavelength optical storage applications.

4.1 Transmittance, reflectance, and absorptance

For a single homogeneous and isotropic layer bounded by isotropic and homogeneous layers, the structure can be described by[48]

$$n(x) = \begin{cases} n1, & \mathrm{x} < 0, \\ n2, & 0 < \mathrm{x} < \mathrm{d}, \\ n3, & \mathrm{d} < \mathrm{x}. \end{cases} \qquad (4\text{-}1)$$

where *n1,n2,*and *n3* are the indices of refraction of medium 1,2,and 3.

As shown in Fig. 4-1, if the plane wave propagates from the left, the electric field vector E(x) can be described using the form:

$$E(x) = \begin{cases} Me^{-ik_{1x}x} + Ne^{ik_{1x}x}, & x < 0, \\ Ce^{-ik_{2x}x} + De^{ik_{2x}x}, & 0 < x < d, \\ Fe^{-ik_{3x}(x-d)}, & d < x, \end{cases} \qquad (4\text{-}2)$$

where *M,N,C,D,* and *F* are the complex amplitudes.

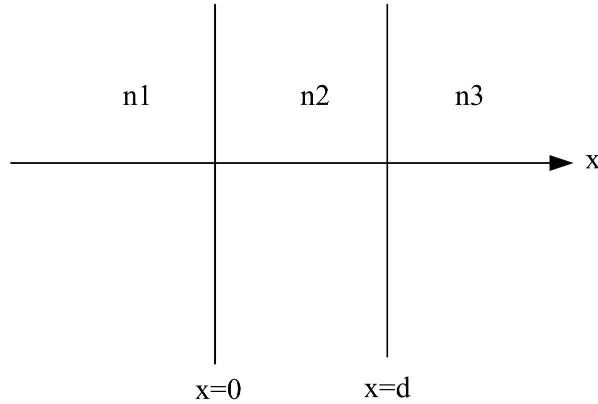

Fig.4-1 A thin homogenous layer of dielectric material

Assume the electric field vector is TE(s) polarized (the electric field is perpendicular to the plane of incidence), and then the complex amplitudes of the incident wave and the reflected and transmitted waves *M*, *N*, *F* are constant. k_{ix} is the x components of the wave vectors:

$$k_{ix} = \left[\left(\frac{n_i w}{c}\right)^2 - \beta^2\right]^{1/2} = \left(\frac{w}{c}\right) n_i \cos\theta_i, \quad i=1, 2, 3, \tag{4-3}$$

where θ_i is the ray angle measured from the x axis. *w* is the angular frequency and c is the speed of light in vacuum. The magnetic field can be obtained from the equation:

$$H = \frac{i}{wu} \nabla \times E. \tag{4-4}$$

From the boundary conditions of Maxwell's equations, the tangential component of the electric and magnetic vectors are continuous across a discontinuity surface[49], so that the electric vector has the same value in each dielectric layer. Using the conditions and Snell's law, the Fresnel reflection and transmission coefficients of the dielectric interfaces for TE wave can be written as[50-52]:

$$r_{12} = \frac{n_1 \cos\theta_1 - n_2 \cos\theta_2}{n_1 \cos\theta_1 + n_2 \cos\theta_2}, \tag{4-5}$$

$$t_{12} = \frac{2n_1 \cos\theta_1}{n_1 \cos\theta_1 + n_2 \cos\theta_2}, \tag{4-6}$$

$$r_{23}=\frac{n_2\cos\theta_2-n_3\cos\theta_3}{n_2\cos\theta_2+n_3\cos\theta_3}\ ,\qquad (4\text{-}7)$$

$$t_{23}=\frac{2n_2\cos\theta_2}{n_2\cos\theta_2+n_3\cos\theta_3}\ ,\qquad (4\text{-}8)$$

respectively.

And the transmission and reflection coefficients can be written as

$$t=\frac{t_{12}t_{23}e^{-i\phi}}{1+r_{12}r_{23}e^{-2i\phi}}\ ,\qquad (4\text{-}9)$$

$$r=\frac{r_{12}+r_{23}e^{-2i\phi}}{1+r_{12}r_{23}e^{-2i\phi}}\ ,\qquad (4\text{-}10)$$

respectively.

The parameter ψ in (4-9) and (4-10) is given by

$$\phi=k_{2x}\,d=\frac{2\pi d}{\lambda}n_2\cos\theta_2\qquad (4\text{-}11)$$

and is proportional to the thickness d and index n_2 of the layer.The expression for the transmission and reflection coefficients of the TM(p) wave are the same, except the coefficients t_{12}, t_{23} and r_{12}, r_{23} must be those associated with the TM waves.

If media 1 and 3 are no absorbing, reflectance (R) defined as the energy reflected from the dielectric structure and transmittance (T) are given by

$$R=|r|^2,\qquad (4\text{-}12)$$

$$T=\frac{n_3\cos\theta_3}{n_1\cos\theta_1}|t|^2.\qquad (4\text{-}13)$$

Regardless of whether the layer (medium 2) is absorbive, both Eqs. (4-12) and (4-13) can be used. Absorptance (A)defined as the fraction of energy dissipated is given by

$$A = 1 - R - T.\qquad (4\text{-}14)$$

Under different angle of incidence, TE and TM states do not behave in the same way, In particular, if the incident angle is at a specific angle, so-called Brewster angle, the reflection coefficient of the TM mode will vanish completely, leaving the reflected light to be TE mode. The Brewster angle, noted as θ_B, is given by

$$\tan\theta_B = n_t / n_i \quad (4\text{-}15)$$

where n_t is the refractive index of the thin film and n_i is the material/air index from the incident side.

4.2 2 x 2 matrix formulation for a thin film

The proper thickness of TE mode can be determined by the matrix formulation. As shown in Fig. 4-2, the electric field E(x) consists of a right-propagating and left-propagating waves can be expressed as the form:

$$E(X) \equiv A(x) + B(x), \quad (4\text{-}16)$$

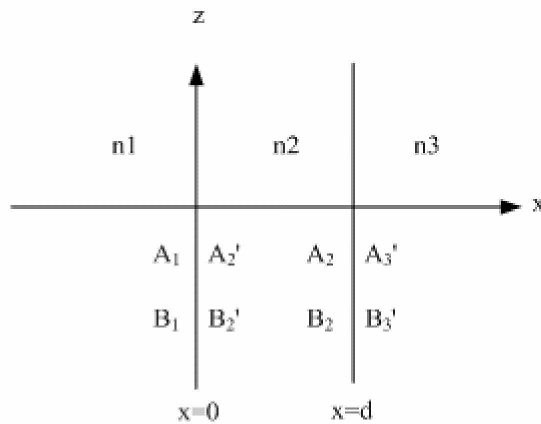

Fig.4-2 A thin layer of dielectric material

Let A(x) represent the amplitude of the right right-traveling wave and B(x) be that of the left-traveling one. To illustrate the matrix method, we define

$$A_1=A(0^-),\ B_1=B(0^-),\ A_{2'}=A(0^+),\ B_{2'}=B(0^+),$$

$$A_2=A(d^-),\ B_2=B(d^-),\ A_{3'}=A(d^+),\ \text{and}\ B_{3'}=B(d^+),$$

where 0^- represents the left side of the interface, x=0, and 0^+ represents the right side of the same interface. Similarly, d^- and d^+ are defined for the interface at x=d.

The transmission matrices that link the amplitudes of the waves on the two sides of the interfaces, noted D_{12} and D_{23}, can be expressed by

$$D_{12} = \begin{pmatrix} \frac{1}{2}\left(1+\frac{k_{2x}}{k_{1x}}\right) & \frac{1}{2}\left(1-\frac{k_{2x}}{k_{1x}}\right) \\ \frac{1}{2}\left(1-\frac{k_{2x}}{k_{1x}}\right) & \frac{1}{2}\left(1+\frac{k_{2x}}{k_{1x}}\right) \end{pmatrix} \quad \text{for TE wave} \tag{4-17}$$

and

$$D_{12} = \begin{pmatrix} \frac{1}{2}\left(1+\frac{n_2^2 k_{1x}}{n_1^2 k_{2x}}\right) & \frac{1}{2}\left(1-\frac{n_2^2 k_{1x}}{n_1^2 k_{2x}}\right) \\ \frac{1}{2}\left(1-\frac{n_2^2 k_{1x}}{n_1^2 k_{2x}}\right) & \frac{1}{2}\left(1+\frac{n_2^2 k_{1x}}{n_1^2 k_{2x}}\right) \end{pmatrix} \quad \text{for TM wave.} \tag{4-18}$$

The expression for D_{23} is similar to those of D_{12}, except that the subscript indices have to be replaced with 2 and 3. Equations (4-17) and (4-18) can be written formally as

$$D_{12} = \frac{1}{t_{12}}\begin{pmatrix} 1 & r_{12} \\ r_{12} & 1 \end{pmatrix} \equiv D_1^{-1} D_2 \tag{4-19}$$

where t_{12} and r_{12} are the Fresnel transmission and reflection coefficients, respectively, and are given by

$$r_{12} = \begin{cases} \dfrac{k_{1x} - k_{2x}}{k_{1x} + k_{2x}} & \text{for TE wave} \\[2ex] \dfrac{n_1^2 k_{2x} - n_2^2 k_{1x}}{n_1^2 k_{2x} + n_2^2 k_{1x}} & \text{for TM wave} \end{cases} \tag{4-20}$$

and

$$t_{12} = \begin{cases} \dfrac{2k_{1x}}{k_{1x} + k_{2x}} & \text{for TE wave} \\[2ex] \dfrac{2n_1^2 k_{2x}}{n_1^2 k_{2x} + n_2^2 k_{1x}} & \text{for TM wave} \end{cases} \tag{4-21}$$

respectively.

where $k_{\alpha x} = n_\alpha \dfrac{w}{c} \cos\theta_\alpha$. (4-22)

Then the amplitudes A_1, B_1 and $A_3^{'}$, $B_3^{'}$ are related by

$$\begin{pmatrix} A_1 \\ B_1 \end{pmatrix} = D_1^{-1} D_2 P_2 D_2^{-1} D_3 \begin{pmatrix} A_3^{'} \\ B_3^{'} \end{pmatrix} \tag{2-23}$$

where D_1, D_2, and D_3 are the dynamical matrices given by

$$D_\alpha = \begin{cases} \begin{pmatrix} 1 & 1 \\ n_\alpha \cos\theta_\alpha & -n_\alpha \cos\theta_\alpha \end{pmatrix} & \text{for TE wave,} \\ \begin{pmatrix} \cos\theta_\alpha & \cos\theta_\alpha \\ n_\alpha & -n_\alpha \end{pmatrix} & \text{for TM wave,} \end{cases} \tag{4-24}$$

where θ_α is the ray angle in each layer and is related to β and $k_{\alpha x}$ by

$$\beta = n_\alpha \frac{w}{c} \sin\theta_\alpha , \tag{4-25}$$

and P_2 is the so-called propagation matrix, which accounts for propagation through the bulk of the layer

$$P_2 = \begin{pmatrix} e^{i\phi_2} & 0 \\ 0 & e^{-i\phi_2} \end{pmatrix} \tag{4-26}$$

and ϕ_2 is given by $\phi_2 = k_{2x} d$. (4-27)

The column vectors representing the plane-wave amplitudes in each layer are related by a product of 2×2 matrices in sequence. A dynamical and propagation matrix can represent each side of an interface and the bulk of each layer, respectively.

We now recall the scheme of Fig. 4-2, with a collimated incident light of wavelength λ , according to Equation (4-23), the characteristic matrix of a thin dielectric film of thickness x is given by

$M[x] =$

$$\begin{bmatrix} \cos\left(\frac{2\pi}{\lambda} n_f x \cos(\theta_f)\right) & -\frac{i}{p_f} \sin\left(\frac{2\pi}{\lambda} n_f x \cos(\theta_f)\right) \\ -ip_f \sin\left(\frac{2\pi}{\lambda} n_f x \cos(\theta_f)\right) & \cos\left(\frac{2\pi}{\lambda} n_f x \cos(\theta_f)\right) \end{bmatrix} \tag{4-28}$$

where θ_f is the incident angle inside the film, $p_f = \sqrt{(\varepsilon_f / \mu_f)}\cos(\theta_f)$ for TE, $p_f = \sqrt{\mu_f / \varepsilon_f}\cos(\theta_f)$ for TM, and μ_f，ε_f are the permeability and permittivity of the thin film, respectively.

The reflectance R and transmittance T can be determined from M(x). From (4-28), R and T are periodical function of x with the period

$$\Delta x = \frac{\lambda}{2n_f \cos\theta_f} \tag{4-29}$$

4.3 Simulation

The optical design of the SiN/Air/SiN stack is performed by using the characteristic matrix. Each layer is described by a 2×2 matrix according to equation (4-28), which relates to the components of the electric (or magnetic) field along the direction of propagation. The reflectivity, transmissivity and absorption of the stack can be derived from multiplication of the matrix of each layer together.

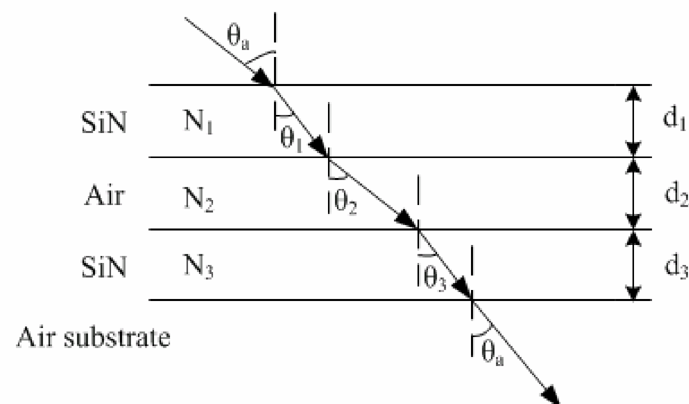

Fig. 4-3. Propagation of an electromagnetic wave through a stack of films of thickness d_i and refractive index N_i.

The characteristic matrix of the stack is given by[51]:

$$M = M_{SiN_1} M_{air} M_{SiN_2} = \begin{bmatrix} B \\ C \end{bmatrix} = \prod_{i=1}^{3} \begin{bmatrix} \cos(\delta_i) & -\frac{i}{\eta_i}\sin(\delta_i) \\ -i\eta_i \sin(\delta_i) & \cos(\delta_i) \end{bmatrix} \begin{bmatrix} 1 \\ \eta_a \end{bmatrix} \tag{4-30}$$

where

$$\delta_i = \frac{2\pi}{\lambda} N_i d_i \cos(\theta_i) \tag{4-31}$$

δ_i is related to the complex refractive index N_i, the thickness d_i of the layers, wavelength λ, and the refraction angle θ_i as shown in Fig. 4-3. The optical admittances, η_i of the i-th layer and η_a of the air substrate are given by

$$\eta_i = N_i \cos\theta_i \quad \text{for TE Mode} \tag{4-32}$$

$$\eta_a = \cos\theta_a \quad \text{for TE Mode} \tag{4-33}$$

$$\eta_i = N_i / \cos\theta_i \quad \text{for TM Mode} \tag{4-34}$$

$$\eta_a = 1/\cos\theta_a \quad \text{for TM Mode} \tag{4-35}$$

The reflectivity R, transmissivity T and absorption A of the incident light for both polarizations can be derived from Eqs. (4-30)~(4-35):

$$R = \left(\frac{\eta_a B - C}{\eta_a B + C}\right)^2, \quad T = \frac{4\eta_a R_e(\eta_a)}{(\eta_a B + C)(\eta_a B + C)^*}, \quad A = \frac{4\eta_a R_e(BC^* - \eta_a)}{(\eta_a B + C)^2} \tag{4-36}$$

If R_{TE} and T_{TE} are the reflectivity and transmissivity for the TE mode, and R_{TM} and T_{TM} for the TM mode, respectively, the optical characteristics of the micro PBS can be evaluated by two extinction ratios σ_T (for transmission) and σ_R (for reflection) defined as

$$\sigma_T = 10 \times \log_{10}\left(\frac{T_{TM}}{T_{TE}}\right), \qquad \sigma_R = 10 \times \log_{10}\left(\frac{R_{TE}}{R_{TM}}\right) \tag{4-37}$$

Our target is to design a PBS with extinction ratios for the transmitted light to be above 10, and for the reflected light to be above 20. From Eqs. (4-30) to (3-37), we

calculated the optical performance of the stack at Brewster angle incidence as a function of d_1, d_2 and d_3, which were the thicknesses of the first silicon nitride layer, the air gap and the second silicon nitride layer, respectively. At Brewster angle incidence, the nominal reflectivity of the TM mode is zero. Therefore, to achieve high polarization extinction ratios, the reflectivity to transmissivity ratio of TE should be as high as possible. Besides, to reduce the fabrication complexity of the micro optical pickup, the thickness, d_1, of the first silicon nitride layer is fixed to be 384 nm, which is the thickness of other micro optical elements. For example, the diffraction efficiency ratio of the 0th order beam and the ±1st order beams could be well controlled within 4~10 at this thickness for a micro-grating in the optical pickup using the three beam tracking method. The index of refraction of low-stress silicon nitride is n=2.189+0.095i at wavelength=405 nm. (The fabrication and optical characteristic of current low-stress silicon nitride will be described in section 4-4.)

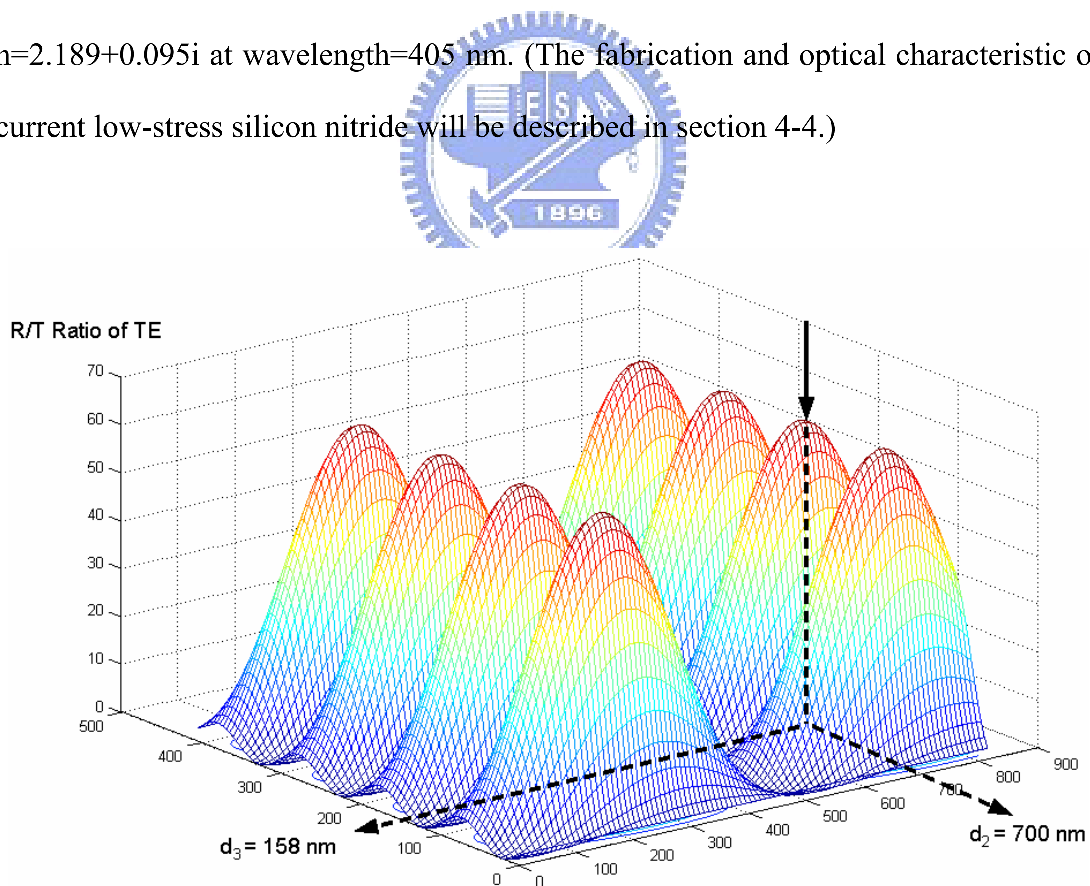

Fig. 4-4. Calculated reflectivity to transmissivity ratio of the TE mode

as a function of d_2 and d_3 at the Brewster angle incidence.

As shown in Fig. 4-4, the reflectivity to transmissivity ratio of the TE mode can be over 50 around the points: (d_2, d_3) = (210 nm, 52 nm), (210 nm, 158 nm), (210 nm, 216 nm), (210 nm, 360 nm), (700 nm,52 nm), (700 nm, 158 nm), (700 nm, 216 nm), and (700 nm, 360 nm). If d_3 was selected to be 52 nm, the mechanical strength of the second silicon nitride film would be too low. On the contrary, if d_3 was selected to be thicker, the absorption for the transmitted light would increase.

Therefore, d_2 and d_3 were selected to be 700 nm to effectively minimize stiction and 158 nm to have adequate mechanical strength, respectively. The calculation also shows that σ_T=15±5 and σ_R=infinity can be achieved at d_1=384±10 nm, d_2=700±100 nm and d_3=152 ± 30 nm. The process margin is also practical in current fabrication technology.

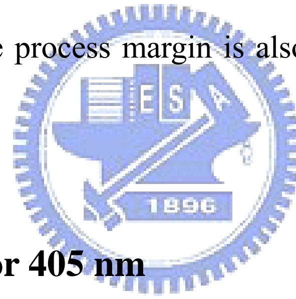

4.4 Silicon nitride film for 405 nm

Silicon nitride can be deposited by the chemical vapor deposition with plasma enhancement (PECVD) or at low pressure (LPCVD). A stress-free PECVD silicon nitride film with high transparency at short wavelength can be obtained by a proper choice of process parameters, such as temperature and gas mixture, etc.[53] The most serious concern of PECVD silicon nitride is its poor chemical durability in HF solution, which is used to remove the sacrificial silicon dioxide layers[54]. The process results in high surface roughness and thickness variation, which will induce distorted waterfronts. As compared with PECVD silicon nitride, LPCVD silicon nitride has higher chemical durability against HF solution. To apply for short wavelength, LPCVD silicon nitride has to possess other two characteristics: lower stress to reduce

curvature and lower absorption to enhance the optical utilization efficiency.

To reduce the thermal stress on silicon based materials, the LPCVD silicon nitride (SiN_x) can be silicon-rich by controlling the gas flow ratio, $SiH_2Cl_2:NH_3$, to be over 5[55]. Our measurement shows that the transparency of LPCVD silicon-rich SiN_x is rather lower for its extinction coefficient k at 405 nm is as high as 0.07. According to Gardeniers' study[56], the mechanical and optical characteristics of the LPCVD SiN_x films are related to the following parameters, in decreasing order of importance: the gas flow ratio of Si and N containing precursors, temperature and pressure, etc.

Since the silicon content is related to the high absorption at short wavelength, the effects of gas flow ratio and annealing condition on the residual stress and optical transmission of SiN_x films were studied in our experiment. All SiN_x films were deposited by LPCVD at 850℃ and 180 mTorr with various SiH_2Cl_2/NH_3 ratio (η) under constant total flow rate of 102 sccm. The deposited films were then annealed at 1050℃ in nitrogen gas.

The dependence of the residual stress on the reaction gas ratio, η, for various annealing time is shown in Fig. 4-5(a). The film stress shows a general decreasing trend with increasing SiH_2Cl_2/NH_3 ratio due to the increased silicon content. After annealing, the stress can be either increased or decreased by two competing mechanisms: the stress relaxation within the grain of the film and the film shrinkage due to dehydrogenation[57].

The dependence of the complex refractive index, n + i k, on the reaction gas ratio for various annealing time is shown in Fig. 4-5(b). The n increases nearly linearly with increasing η while the k shows a sharp increase for $\eta > 3$, due to the increased content of silicon with high index and high absorption. For the SiN_x film to be used in the micro PBS, it should be low stress and low absorption. Since higher SiH_2Cl_2/NH_3

ratios decrease the stress but increase the absorption, a trade-off is required. Therefore, a SiH_2Cl_2/ NH_3 ratio = 3 with two-hour annealing was selected to fabricate the lower stress (585 MPa) and lower absorption (n = 2.189+i0.0095) micro PBS.

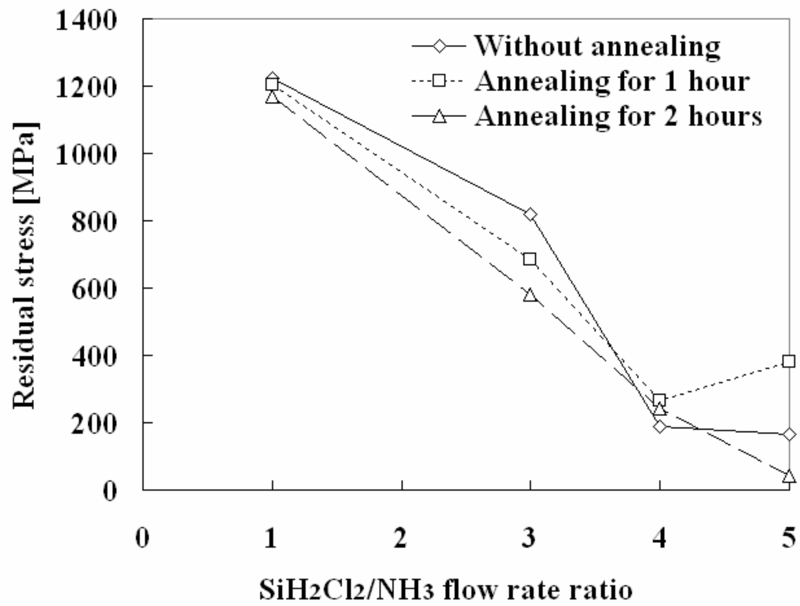

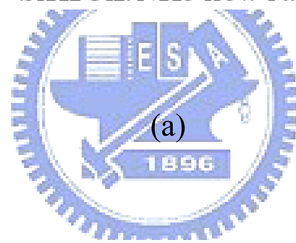

(a)

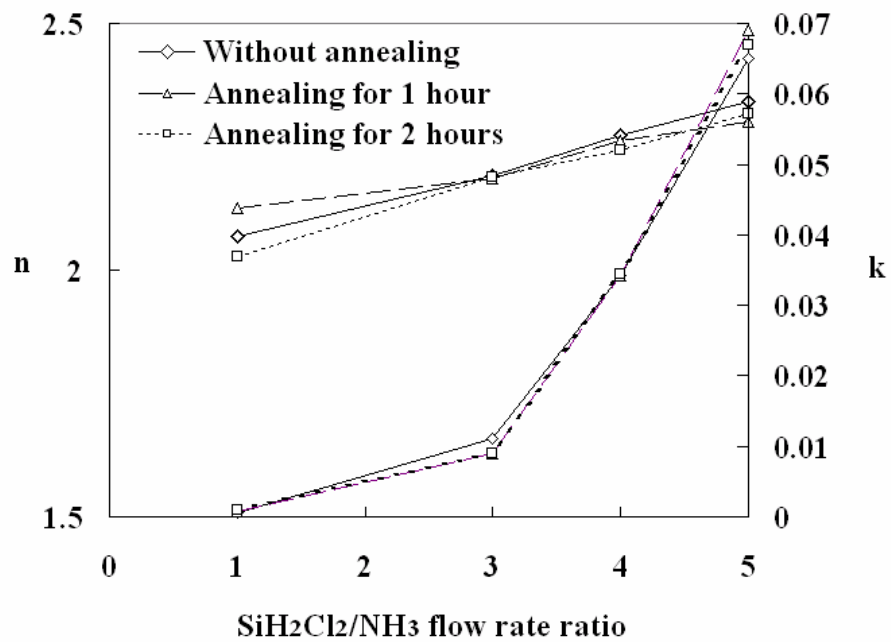

(b)

Fig. 4-5. Dependence of (a) residual stress and (b) complex refractive index, n + ik, on the reaction gas ratio for various annealing times.

4.5 Summary

The optical theory of thin films has been briefly described in this chapter. We presented the fundamental theory and basic design of our stacked PBS. To reduce the fabrication complexity, the PBS consisted of a novel stack of two silicon nitride layers separated by an air gap. The simulation showed that if the thicknesses of the first silicon nitride, air gap and the second silicon nitride were selected to be 384 nm, 700 nm and 158 nm, respectively, the extinction ratios of the PBS would be above 10 for the transmitted light and above 20 for the reflected light.

The development of the low stress silicon nitride film with low absorption at 405 nm was also described. The result showed that using the recipe SiH_2Cl_2/ NH_3 ratio = 3 with two-hour annealing produced a silicon film with lower stress (585 MPa) and low absorption (n = 2.189+i0.0095).

Chapter 5

Fabrication and Measurement of a Polarization Beam Splitter

5.1 Structure design and device fabrication

The stack of two silicon nitride layers separated by an air gap can be fabricated by surface micromachining. The structure is shown in Fig. 5-1. A poly silicon capping ring is used to mount a stack of silicon dioxide and silicon nitride layers, which are deposited alternatively on the poly silicon frame. After HF solution releasing, the silicon dioxide layers are removed, leaving an air gap, whose height can be controlled by dimples.

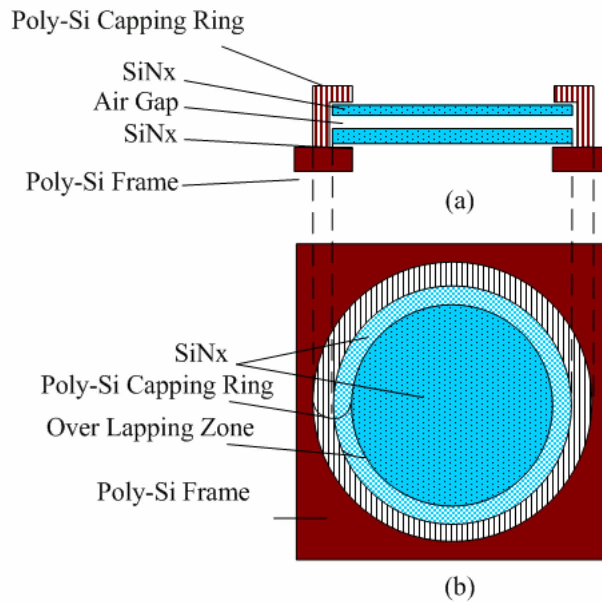

Fig. 5-1. Schematic of the micro PBS: (a) cross-sectional and (b) top view.

As compared with the previous surface micromachining, which we use to make the multi-beam optical pickup, there are some differences. First, there are two silicon nitride layers and one silicon dioxide sacrifical film after the first poly-silicon structural layer. Besides, there is no metal layer in the fabrication of the micro-PBS. The surface micromachining we use to make a pop-up type micro PBS is illustrated in Figure 5-2. The three-dimensional micro PBS consists of two layers of SiN_x optical film mounted in a poly-Si supporting frame. The support frame is held perpendicular to the substrate by locking with a micro-spring latch. To fabricate the device, a sacrificial silicon dioxide (SiO_2) layer was first deposited on the silicon substrate. Dimples and first anchors were then patterned in the sacrificial layer (Fig. 5-2a). The first structural poly-Si was deposited by LPCVD and patterned to form a micro-frame. (Fig. 5-2b). A SiO_2 layer and the first optical SiN_x layer were deposited and patterned (Fig. 5-2c).. After depositing a SiO_2 layer, a 0.7-um-deep dimple array was etched to

control the air gap after releasing. The second optical SiN_x layer was deposited and patterned before depositing a SiO_2 layer (Fig. 5-2d).. Both SiN_x layers were deposited aiming for a thickness slightly greater than the target value. The thickness was further reduced to the target value at the HF releasing step. After patterning another anchors, the second structural poly-Si layer was deposited and patterned to implement the micro-spring latches and the micro-frame (Figure 5-2e). The wafer was annealed for two hours at 1050℃ in nitrogen to reduce the residual film stress. After releasing in HF solution (Fig. 5-2f), the micro PBS was then lifted to its vertical position by using a micro-probe, (Fig. 5-2g). The SEM micrographs of a pop-up micro PBS with a central aperture of 500 μm in diameter is shown in Fig. 5-3(a). Using the same process, the micro PBS was integrated with other components to form a micro optical pickup as shown in Fig. 5-3(b).

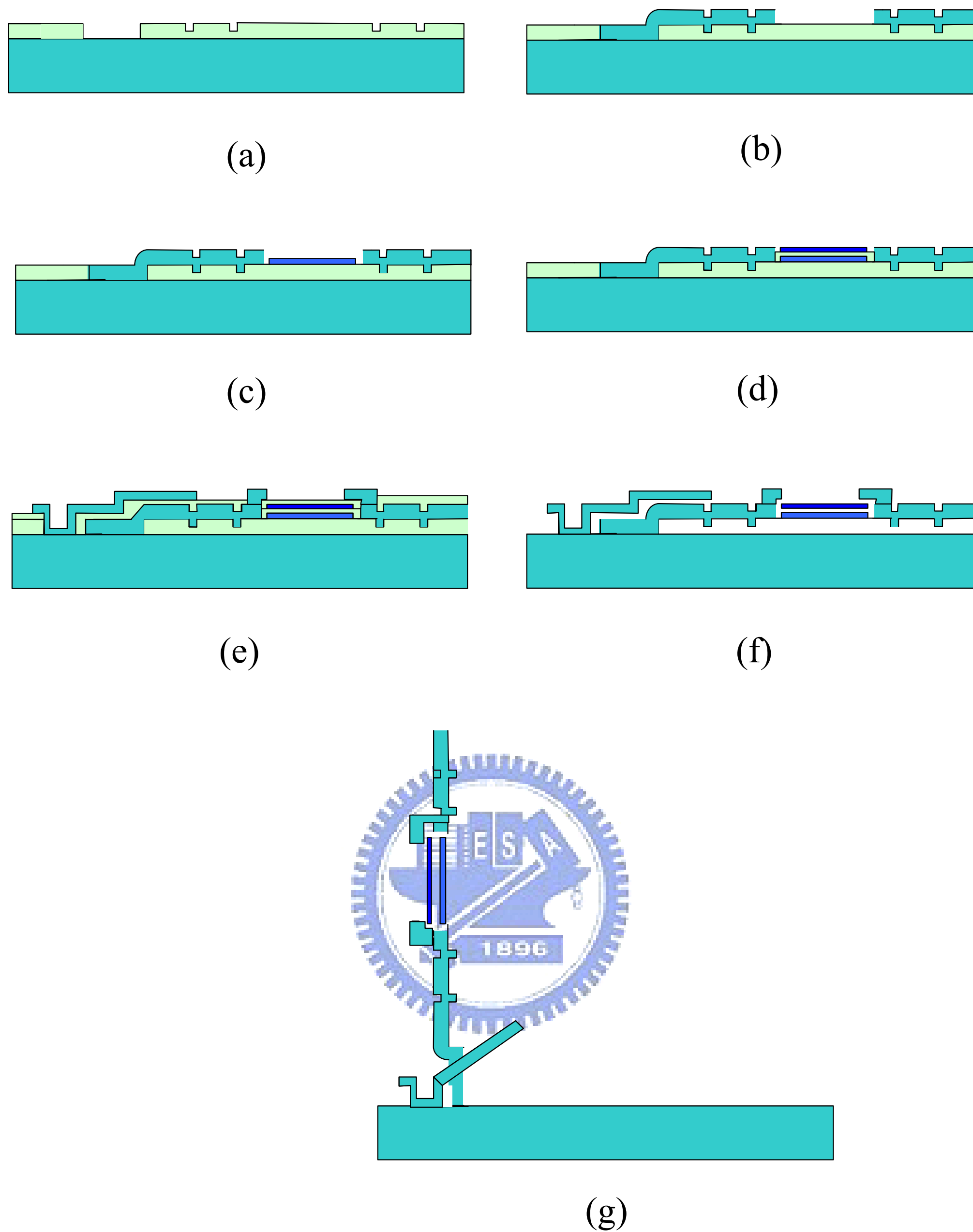

Fig. 5-2. Cross section of the processing sequence for fabricating the micro PBS: (a) definition of dimples and anchors, (b) definition of the first poly-silicon layer. (c) definition of the first silicon nitride layer, (d) definition of the second silicon nitride and the second poly-silicon layer, (e) the structure after HF release, (f) the pop-up micro-structure.

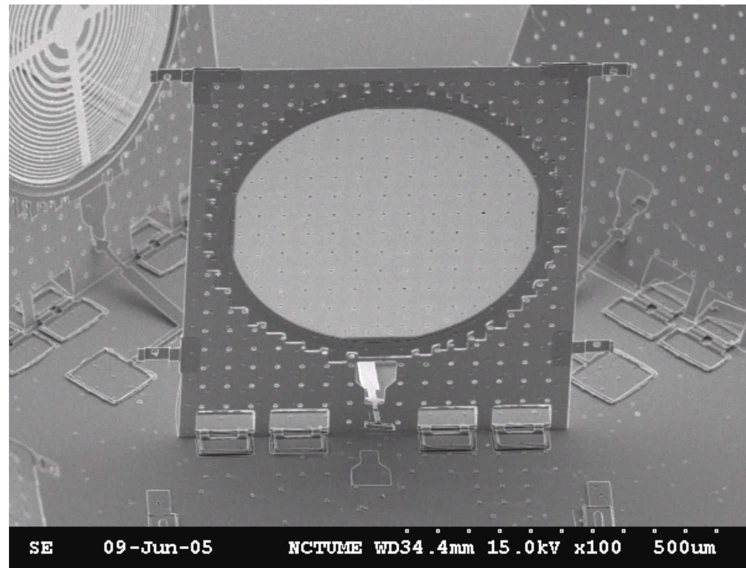

(a)

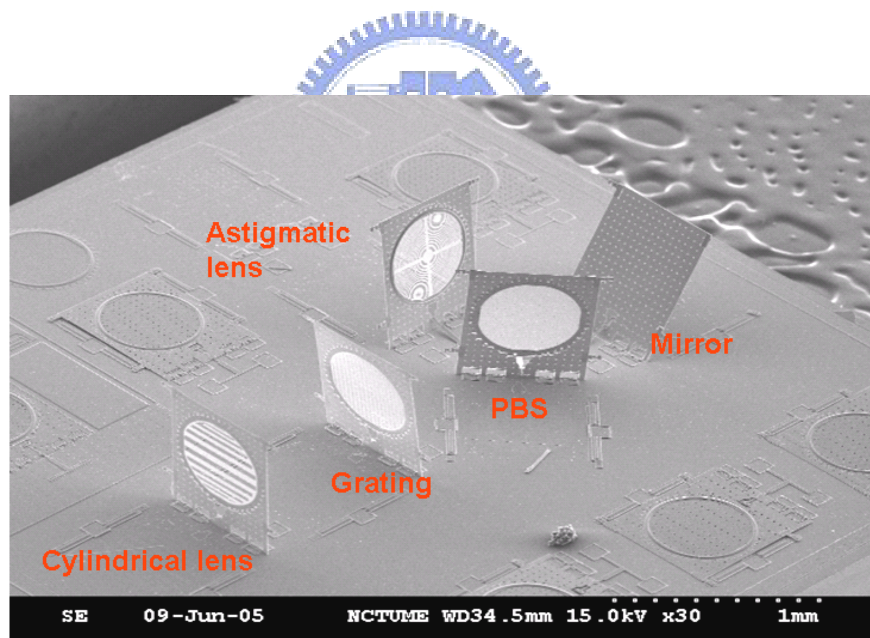

(b)

Fig. 5-3. SEM photographs of (a) the micro pop-up PBS and (b) a micro optical pickup, including a cylindrical lens, a grating, a PBS a folded mirror and an astigmatic lens.

5.2 Experimental results and discussions

To measure the optical characteristic of the micro PBS, a GaN semiconductor laser at λ=405 nm was used as the light source. A retarder and a polarizer were used to adjust the polarization state of the light. An aperture of a diameter 200 μm was used to yield the beam size comparable with the micro PBS at Brewster angle incidence. The beam profile was measured by a CCD camera positioned at 10 mm from the micro PBS. The configuration used for measuring optical properties of micro-PBS is depicted in Fig.5-4.

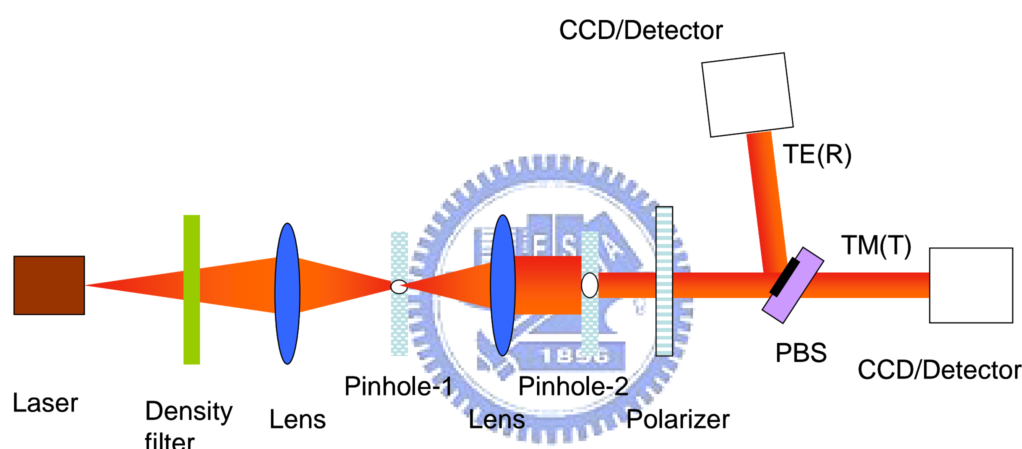

Fig. 5-4 Configuration of the measurement system

In the fabrication of the three-layered optical structure, it is difficult to precisely control the thickness of each layer. One of the cause is the difference of boundary conditions for the first (upper) and the second (lower) silicon nitride layers, as shown in Fig. 5-5. The upper silicon nitride is between air and the silicon dioxide, while the lower silicon nitride is between two silicon dioxide layers. The difference will induce the different etch rate to the silicon nitride layers.

The beam profiles of TE mode before and after reflecting from the micro-PBS are

shown in Fig. 5-6 (a). The peak reflectivity and transmissivity were measured to be 93% and 2.8 % of the incidence, respectively, while the absorption and scattering loss were 4.2% together. After reflection, the spot shape became changed obviously, which was caused by the stress-induced curvature of the micro PBS. The beam profiles of TM mode before and after transmitting through the micro-PBS are shown in Fig. 5-6 (b). The peak reflectivity and transmissivity were measured to be 0.3% and 85 % of the incidence, respectively, while the absorption and scattering loss were 14.7 % together. The measurement data are summarized in Table 5-1. σ_T=15 dB is close to the calculated value of 18, while the σ_R is as high as 25 dB. Both values match our design specification, σ_T >10 andσ_R >20, while the deviation was due to the scattering loss from the dimples, etch holes and surface roughness, 30 nm rms. A lower absorptive and lower stress silicon nitride can potentially yield a higher-extinction-ratio micro PBS using the similar processes for more demanding applications.

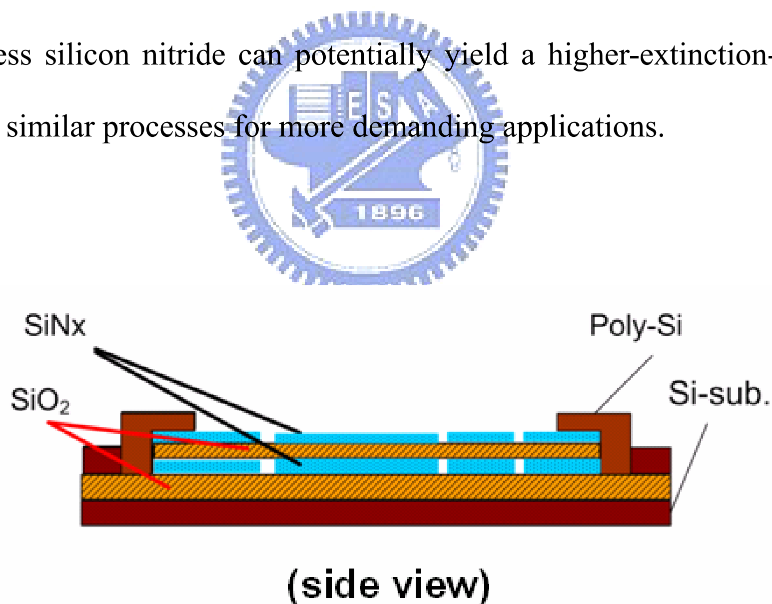

Fig. 5-5 Schematic of the cross view of the beam splitter.

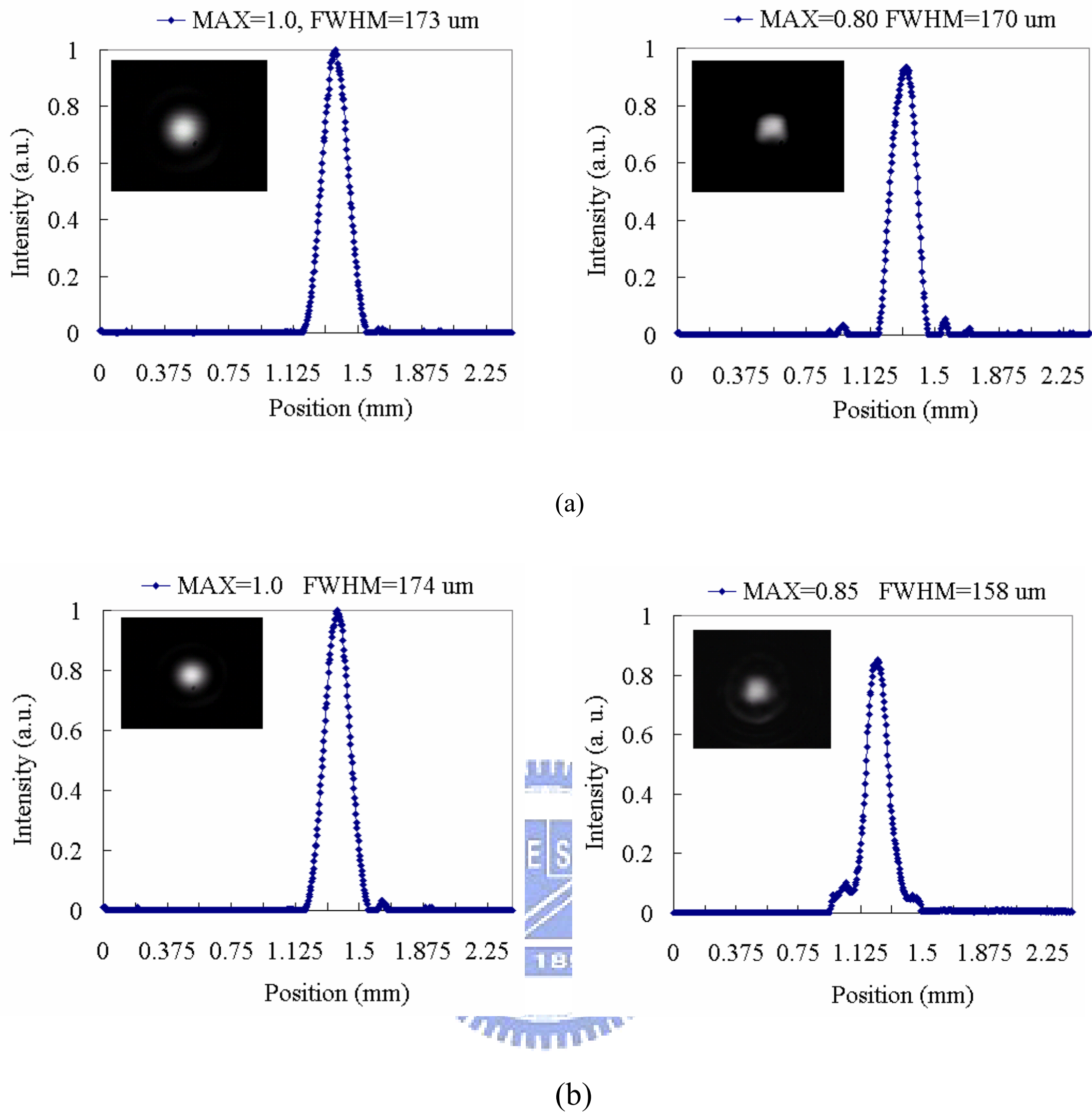

Fig. 5-6. (a) Beam profiles of TE mode before (left) and after (right) reflecting from the micro-PBS. (b) Beam profiles of TM mode before (left) and after (right) transmitting through the micro PBS.

Table 5-1. Optical performance of the pop-up micro PBS at Brewster angle incidence

	Calculation	**Measurement**
Reflectance of TE (%)	96	93
Transmittance of TE (%)	1.5	2.8
Reflectance of TM (%)	0	0.3
Transmittance of TM (%)	86	85
σ_T (dB)	18	15
σ_R (dB)	Infinite	25

5.3 Comparisons

A comparison of the planar and current pop-up polarization beam splitters is listed in table 5-2. The two planar types are single-layered, which is designed for longer wavelength 633 nm. The current pop-up type is three-layered, which is designed for shorter wavelength 405 nm. The reflectance of the TE mode of the pop-up type is higher than that of the two planar types. Because of the high absorption and scattering loss, the transmittance of the TM mode of the pop-up type is lower than that of the two planar types. Considering the extinction ratio, the three-layer pop up structure is higher.

Table 5-2: Comparison of planar and pop-up polarization beam splitters

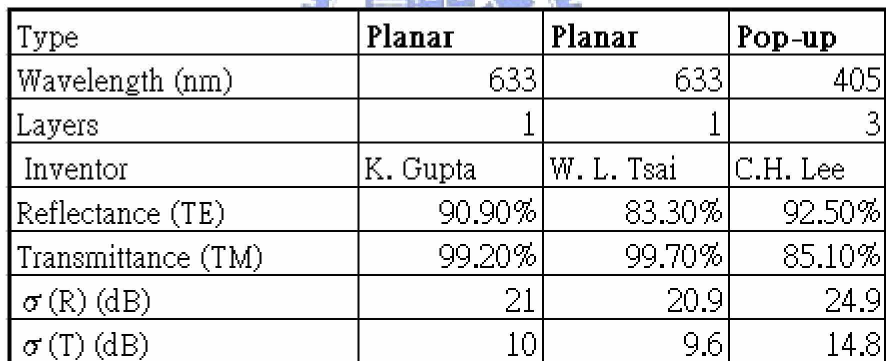

Type	**Planar**	**Planar**	**Pop-up**
Wavelength (nm)	633	633	405
Layers	1	1	3
Inventor	K. Gupta	W. L. Tsai	C.H. Lee
Reflectance (TE)	90.90%	83.30%	92.50%
Transmittance (TM)	99.20%	99.70%	85.10%
σ (R) (dB)	21	20.9	24.9
σ (T) (dB)	10	9.6	14.8

5.4 Summary

A low stress silicon nitride film with low absorption at 405 nm was fabricated with the optimal process parameters. A stack that consists of two such silicon nitride layers separated by an air gap can function as a high polarization extinction-ratio PBS with σ_T=15, σ_R=25. The micro PBS can be integrated with other optical elements to form a micro optical bench for short wavelength optical storage applications.

Chapter 6

Micro Reflective System

In the development of optical pickups, the current trend is towards being CD/DVD/ HD-DVD compatible. To realize this function in a micro-optical pickup, one of the solutions is to use a rotary actuated mirror to assist switching between each light source, as illustrated in Fig. 6-1. However, the maximum rotation angle of the surface micromachined rotary actuator is below 2.5°, which is limited to trwo mechanisms: (a) the mechanical spring exhibits stronger nonlinear effects under high rotation angle, reducing rotation angles at the same voltage biases, and (b) under a larger rotation angle, the stiffness in the angular direction and the compliance in the radial direction occur. Increase the distances between the laser diodes and the rotary actuated mirror is a straightforward way to solve the issue of low rotation angle of the actuator. The side effect is the chip size would be enlarged from 0.2 mm x 0.6 mm to 0.7 mm x 0.6 mm. If the rotation angle can be enhanced to be 10°, the chip size can maintain the same.

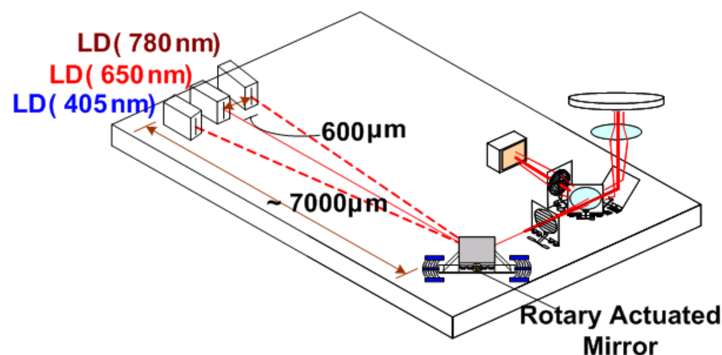

Fig. 6-1. Schematic of a CD/DVD/HD-DVD compatible micro-optical pickup, which uses a rotary actuated mirror to switch between each light source.

In this section, we present the working principle of a micro-reflective system, which possesses the same function of the rotary actuated mirror and produces an equivalent rotation angle larger than 35°. The design concept is based on the rotary motion being equivalent to the combination of the angular to linear conversion and the linear motion. The micro-reflective system is consisted of a prism and a parabolic mirror. The prism is actuated by a linear actuator and used to perform the liner shift of the incident beam, while the parabolic reflector is used to perform the angular to linear conversion. The device is fabricated on a silicon-on-insulator (SOI) platform.

6.1 Optical Design

The micro-planar reflective system (PRS) is integrated with two dimensional waveguides. The design is composed of a parabolic mirror, a prism, and an electro-thermal actuator as illustrated in Fig. 6-2, the parabolic mirror is used to redirect an axially parallel incident beam to its focal point or reflect a beam, which passes through its focal point, back along the axial direction. In Fig. 6-3(a), the geometric shape of the parabolic mirror in a two dimensional waveguide can be expressed as:

$$z=x^2/(4f)$$

where f = 100 μm is the axial focal length in our design. The prism deviates the beam as shown in Fig. 6-3(b). It is a Porro type, which is a right geometric prism with right-angled triangular end faces. Incident beam enters the large rectangular face of the prism at normal angle, undergoes total internal reflection twice from the sloped faces, and exits again through the large rectangular face at normal angle. The lateral displacement between the incident and the exit beams is a function of the incident position and the geometry of the prism.

In operation, the incident light is coupled from a lens fiber into an index guided

waveguide (5 μm wide and 5 μm high). After collimation by a curved mirror, the light passes through the focal point of the parabolic mirror and then reflects from the curved

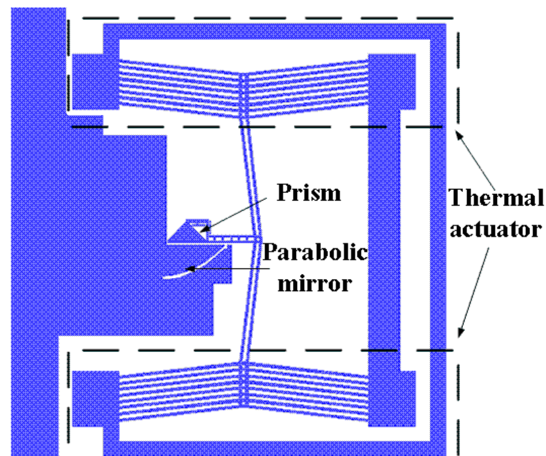

Fig. 6-2. Schematic of the proposed planar microreflective device, which is composed of a parabolic mirror, a prism, and a thermal actuator.

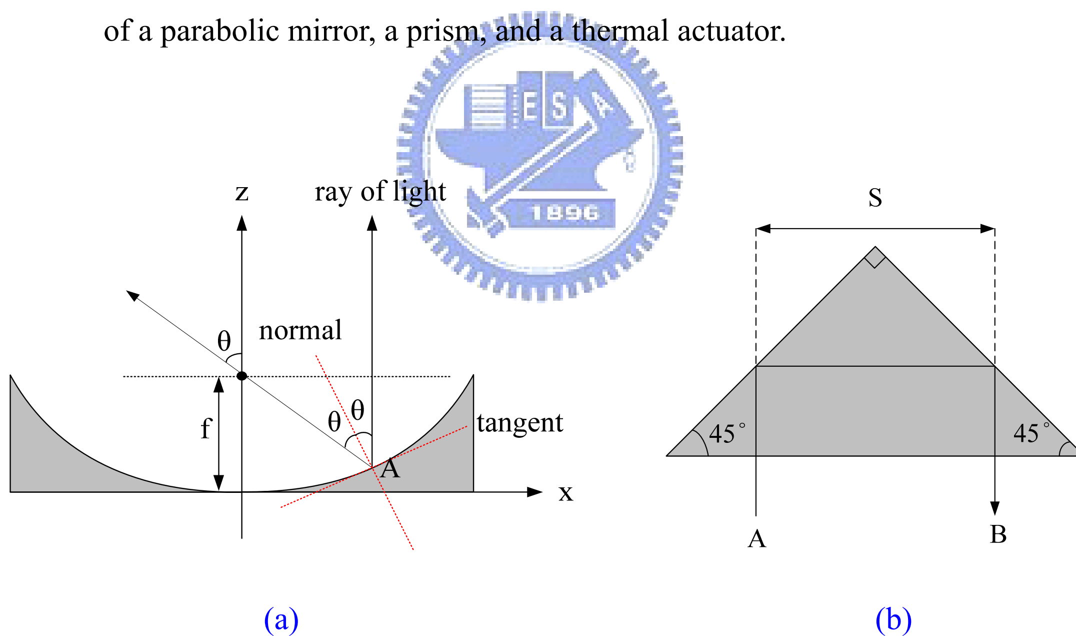

Fig. 6-3. (a) The incident angle, θ, is a function of position of point A and the focal length, f. (b) For an incident beam enters a Porro prism, the displacement, S, is related to the entrance point A.

silicon-air interface of the parabolic mirror. To avoid transmission loss at this interface, the total internal reflection condition is matched. The light then enters the air gap

perpendicular to the Si-air interface. Since larger air gap between the Si-slab and the prism will result in higher diffraction loss, the air gap is designed to be 5 μm. To enhance transmission, an antireflection layer can be coated on the sidewall of the Si-slab. The prism possesses a simple geometry of a 45 degree right triangle with a 136 μm hypotenuse face. In the prism, the light entering the hypotenuse face at a perpendicular angle is reflected twice from the smaller prism faces (or legs) and exists from the hypotenuse face. After reentering the Si-slab, the light is again reflected from the parabolic mirror and redirected to the focal point of the parabolic mirror. The prism position is controlled by an electro-thermal actuator, which is composed of two sets of V-shape electro-thermal beams. If the prism is slightly displaced parallel to the Si-slab, the equivalent reflection angle at the virtual reflection point (the focal point of the parabolic mirror) would be small as shown in Fig. 6-4(a). On the other hand, if the prism is displaced farther, the equivalent reflection angle would be large as shown in Fig. 6-4(b).

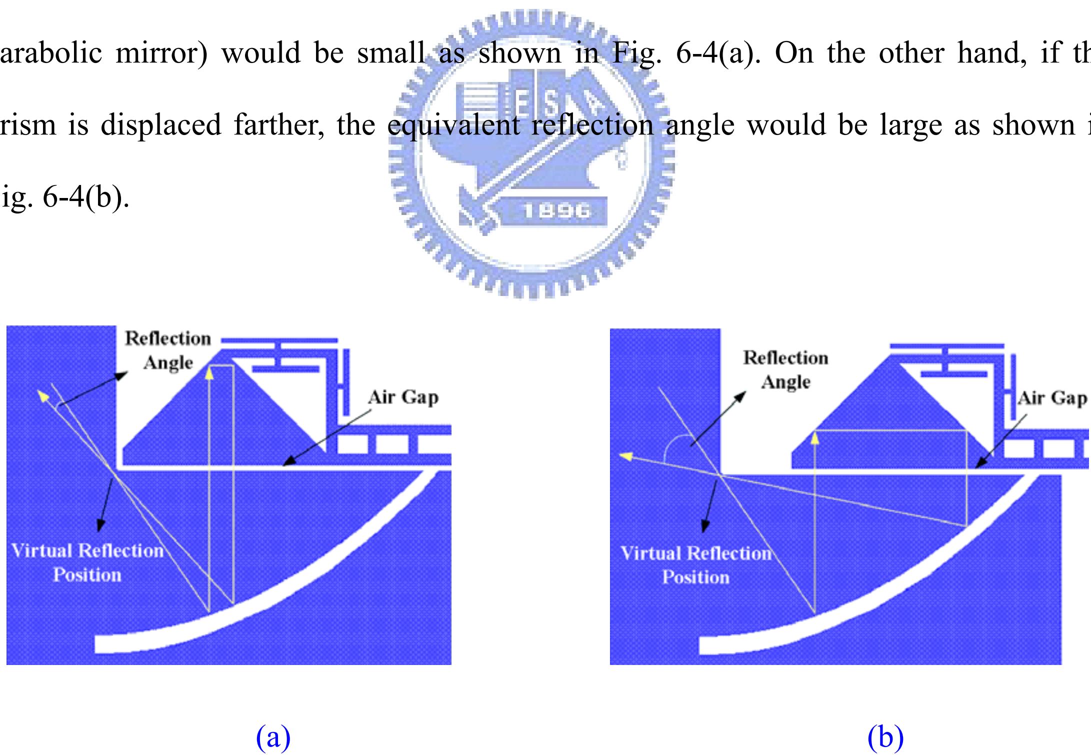

Fig. 6-4. Schematics of (a) small reflection angle produced by small displacement of the prism and (b) large reflection angle produced by large displacement of the prism.

The displacement of the prism is modeled using FEMLAB software's multi-physics analysis, which includes the conductive media, heat transfer, and plane stress models. Sputtered Pt has been used as the heat source, while silicon has been used as the material of the thermal actuator.

6.2 Fabrication

The device was fabricated on a silicon-on-insulator (SOI) wafer with a 5 μm thick silicon device layer and a 2 μm thick buried silicon dioxide layer. The fabrication

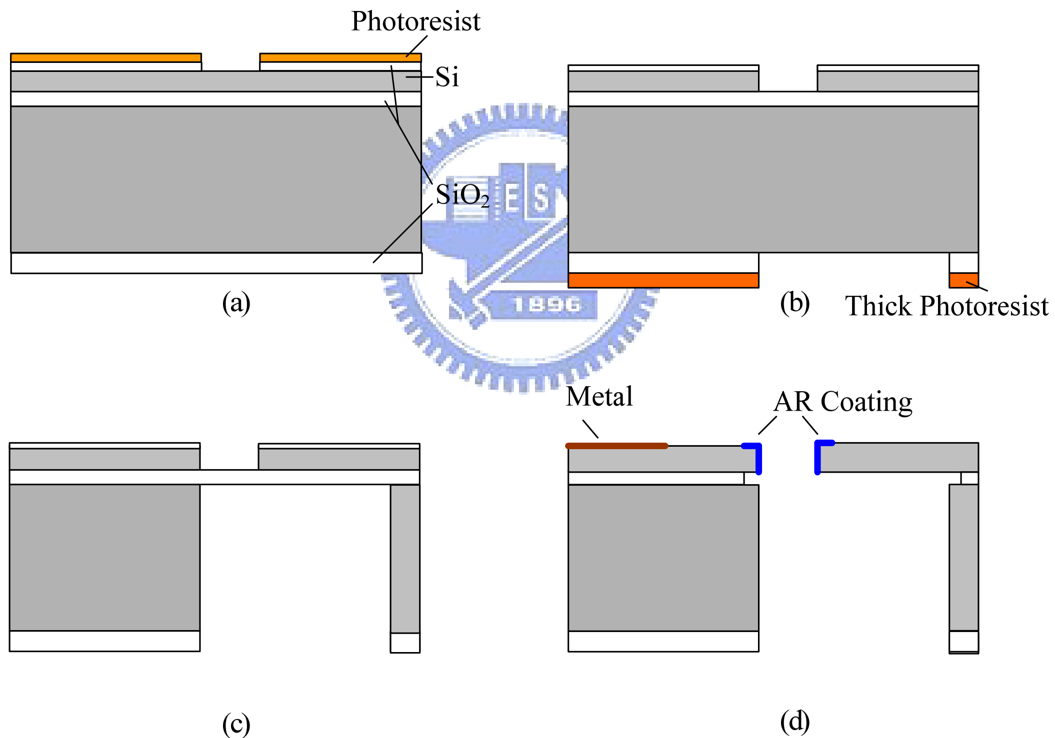

Fig. 6-5. Process flow for the planar micro-reflective device.

process is illustrated in Figure 6-5. A 0.5 μm thick thermal oxide layer on the front-side and a 4-μm thick PECVD oxide layer on the backside were grown as the hard mask for silicon etching. After patterning the waveguides, parabolic mirrors, prisms, and thermal actuators on the front-side, the silicon dioxide was dry etched using fluorine (CHF_3)

based chemistry (step a). After stripping the photoresist, the front-side silicon device layer was dry etched using HBr based chemistry to the buried oxide. The wafer was then dipped in BOE for 1 minute to remove the oxide-like byproduct from the HBr dry etching process. After patterning the backside using thick photoresist, the backside silicon dioxide layer was etched (step b). The backside silicon was etched to the buried oxide layer by a deep reactive ion etching (DRIE) using Bosh process, which consists of cycled etching and passivation steps (step c). The wafer was then released using HF vapor at 40 °C. A shadow mask was used before evaporating the anti-reflection layer, ZrO_2, twice by e-beam under 30° tilting to coat the sidewalls of the Si-slab and the prism, respectively (step d). A composite metal film, 50 Å Ti/ 800 Å Pt, was finally coated as the heat source in the actuator area using another shadow mask. The SEM of the fabricated planar micro-reflective system is shown in Fig. 6-6.

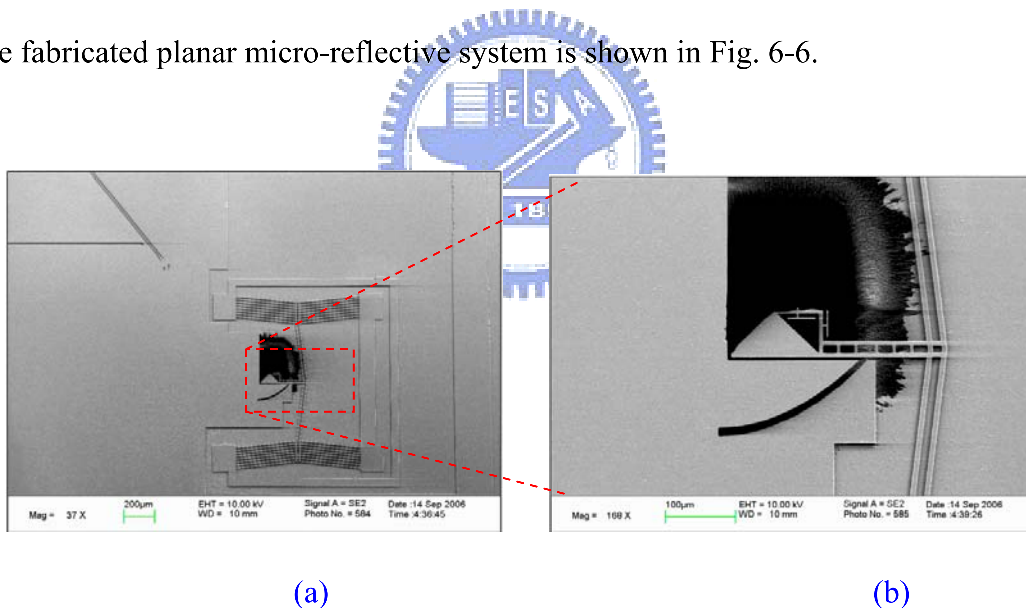

(a) (b)

Fig.6-6. SEM image of the fabricated PRS (a) The entire PRS including the waveguide to guide the incident light. (b) The enlarged view of the prism and the parabolic reflector.

6.3 Experimental Results and Discussion

To measure the optical performance of the microdevices, an input signal (λ=1550 nm,

TE mode) was used. A polarizer and a quarter wave plate were adjusted to obtain the required polarization states. The experimental setup is shown in Fig. 6-7. The beam was coupled into a rectangular waveguide, 5 μm wide and 5 μm high, from a lensed fiber tilted by 45 degrees as shown in Fig. 6-8(a). At the end of the rectangular waveguide was a curved mirror and a plane mirror, which were used to collimate and direct the

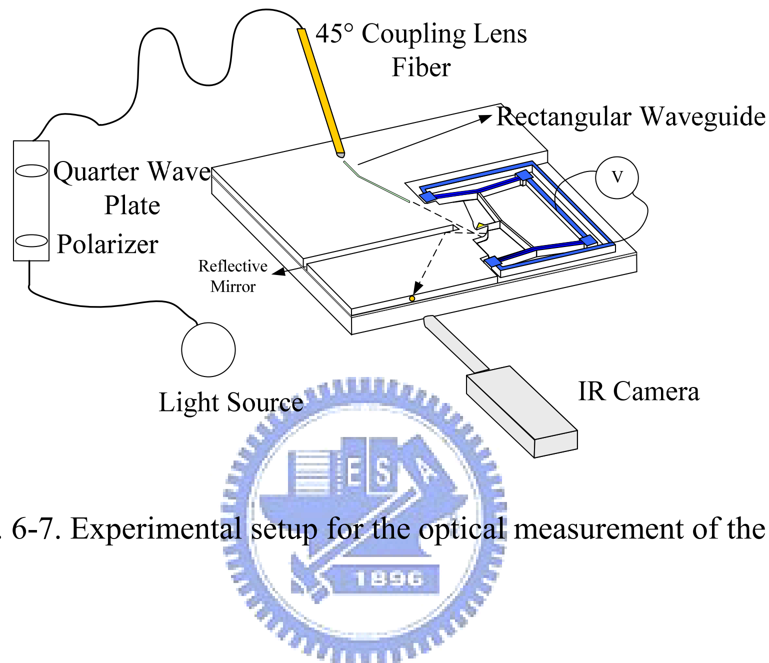

Fig. 6-7. Experimental setup for the optical measurement of the PRS.

beam to the PRS, respectively. The prism of the PRS was actuated by applying a DC bias across the pads of the two V-shape electro-thermal beams to change the optical path of the beam. After outputting from the PRS, the beam was reflected by an air-gap based mirror and redirected to the facet of the chip. Infrared (IR) images of the optical beam were observed at the facet of the chip as shown in Fig. 6-8(b), which verified the dynamic switching capability of the PRS. The reflection angle as a function of displacement of the prism in the PRS is shown in Fig. 6-9. The calculated value is based on the Gaussian beam approximation and geometry of the parabolic mirror and prism. The maximum equivalent scan angle is 38° at a prism displacement of 45 μm. The discrepancy from the calculated value is partly due to the linewidth deviation during the fabrication process and the instability of the electro-thermal actuator under

high temperature.

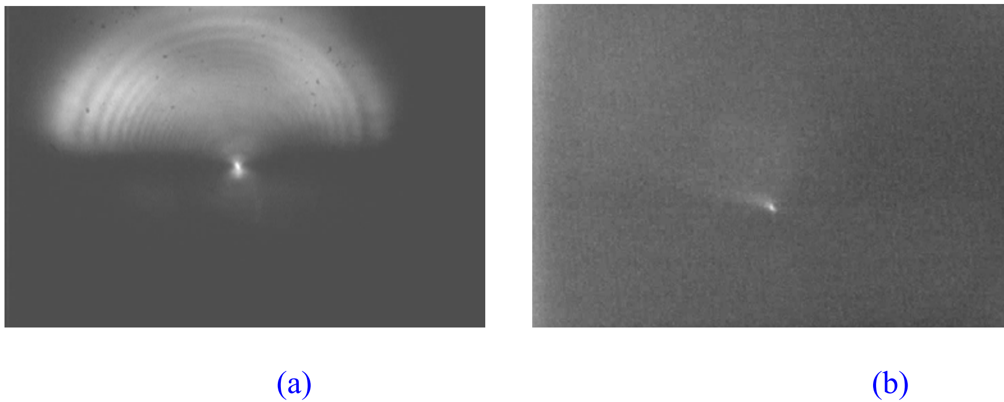

(a) (b)

Fig. 6-8. The infrared near field images of the optical beams at (a) the front end of the rectangular waveguide, which is the input spot; and (b) the facet of the chip, which is the output spot.

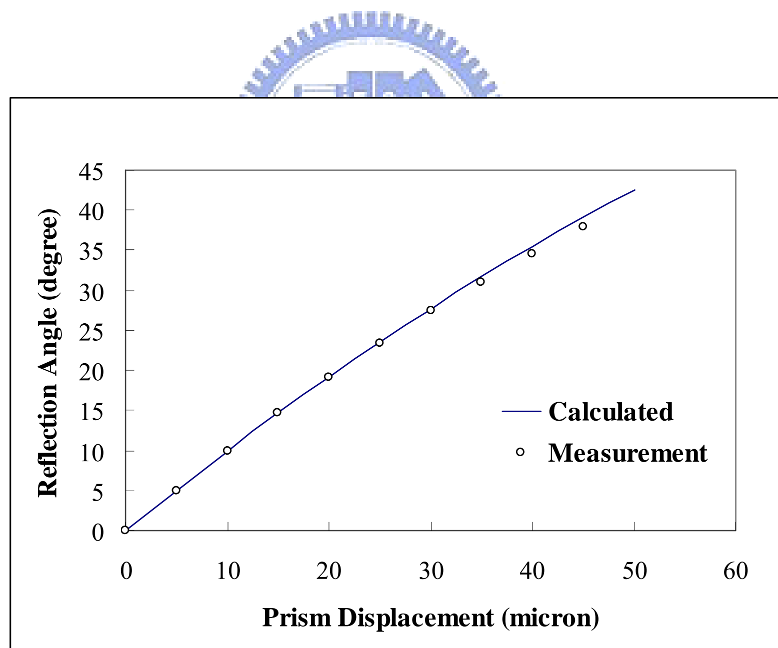

Fig. 6-9. The reflection angle as a function of prism displacement.

The maximum equivalent angle could be increased in principle by designing an actuator with larger displacement. As compared with the previous design proposed by Chi[58], the equivalent scan angle of our device is three times larger. Besides, when

applied in a waveguide system, there are no these drawbacks: (a) the position of the reflection point varies with rotation angle, (b) the rotation angle is reduced when the light beam re-enters the silicon slab, and (c) the larger air gap between the slab and the mirror results in high diffraction loss. The illustration of these drawbacks is shown in Fig. 6-10. The effective rotation angle inside the Si PRS is reduced by n, the refractive index of silicon, according to the Snell's law:

$$\theta_{si} = \sin^{-1}\left(\frac{\sin\theta}{n}\right) \cong \frac{\theta_{air}}{n}$$

The position of the reflection point varies from R1 to R2 as the mirror rotates. The air gap between the Si slab and the mirror also increases with scan angle, which induces high diffraction loss.

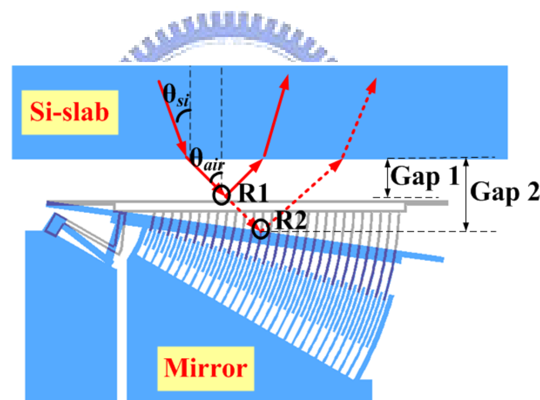

Fig. 6-10. Schematic of the light reentering the silicon slab.

6.4. Summary

Using a parabolic mirror and a prism, the micro reflective system, which reflects the incident beam to large angle under constant air gap and fixed reflection point, has been demonstrated. The maximum equivalent scan angle is 38°, which is almost three times larger as compared with that of conventional micro rotary mirror. The optical

performance of the micro-device shows its potential application in planar waveguide optics. The concept can be also applied in a surface micro-machined pickup to realize a CD/DVD/HD-DVD compatible system. As illustrated in Fig. 6-11, the prism and the parabolic reflector can be replaced with a set of mirrors and a vertical parabolic reflector, respectively.

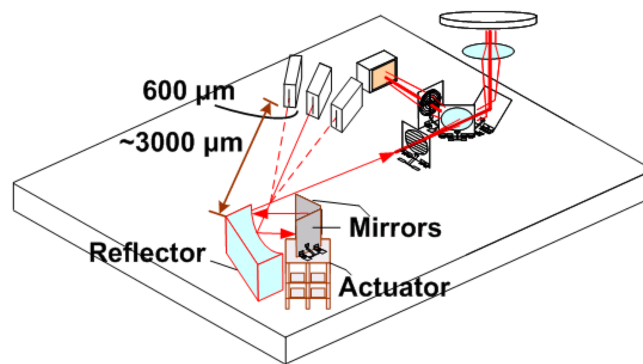

Fig. 6-11. Schematic of a CD/DVD/HD-DVD compatible micro-optical pickup, which uses a surface micro-machined linear actuated mirror and a vertical parabolic reflector to switch between each light source.

Chapter 7

Conclusions and Future Works

7.1 Conclusions

The combination of optics and micro-fabrication technologies has emerged as a new branch of science during the past 10-20 years and is gradually making its way towards commercialization in a number of fields. Because of its capabilities of miniaturization and design flexibility, micro-optical devices have become the key technology for building compact optoelectronic systems.

Micro-optical pickup, a kind of optoelectronic system, has the desired features of compact size, light weight, low power consumption and batch-fabrication. All these properties of micro-optical pickups can fulfill the requirements of the next generation optical storage applications, which are revolutionizing our society.

In this thesis, we demonstrated three novel micromachining devices to be applied in the next generation micro-optical pickups. The first is a micromachined free-space switchable grating, which can be used to realize a multi-beam optical pickup. The second is a stacked micro polarization beam splitter, which can be used with a quarter wave plate to achieve high extinction ratios and realize a high efficiency micro-optical pickup. The third is a planar reflective system, which is consisted of a prism and a parabolic reflector. The concept has a potential to realize a CD/DVD/HD-DVD compatible surface micro-machined optical pickup. Based on these experiences, we propose a new type micro-optical pickup to fully take advantages of the above surface micro-machinined devices in the future work.

7.1.1 Switchable grating in a micro optical pickup

In some conventional optical pickups, using multiple beams in parallel is a straightforward solution to improve the data rate. However, weight, large volume, adding more components and intensive assembly are the main issues of conventional solutions.

In order to improve these drawbacks, we demonstrated a silicon-based micro switchable grating, which can be used to switch between single-beam recording and multi-beam reading. This device was composed of a binary phase grating and a stress-induced actuator. Low stress silicon nitride was used as the optical material of the binary phase grating due to its high transparency in the visible spectrum and its superior chemical and mechanical properties. The switching can be easily controlled using an electrostatically driven stress-induced curved actuator. Furthermore, the actuator and the grating were batch-fabricated using a two-layer poly-silicon and one-layer silicon nitride micro-machining process. The measurement showed that three diffracted beams with nearly equal intensity from the grating were generated when a voltage was applied to the actuator to switch its position. The single-beam and multi-beam configurations can be used for writing and reading optical disc, respectively. By using these well-developed fabrication processes and smart designs, the switchable grating integrated with other micro-optical components on a silicon substrate can be produced economically and reproducibly in large volume.

7.1.2 High-extinction-ratio Polarization Beam Splitter

In some optical pickups, polarizing beam splitters (PBSs) are used with a quarter wave plate to simultaneously produce high TM-mode transmitted light and high TE-mode reflected light. The PBS is usually realized using a larger-size birefringence

crystal or a high-cost films-coated glass. However, in a miniature optical system, it is difficult to realize such a device at low cost and compatible process.

Our proposed high-extinction-ratio PBS possesses the similar function of a conventional bulky PBS. This PBS used low-absorption silicon nitride layers for blue wavelength applications and consisted of novel stack of two silicon nitride layers separated by an air gap. An optimized PBS model was developed to achieve high extinction-ratio for polarized light with an adequate surface micromachining margin. The polarization extinction ratios of 25 dB for the reflected light and 15 dB for the transmitted light were experimentally achieved at λ=405 nm. Furthermore, the fabrication of the PBS is compatible with other diffractive elements and can be used to build up a micro optical bench for short wavelength optical storage applications.

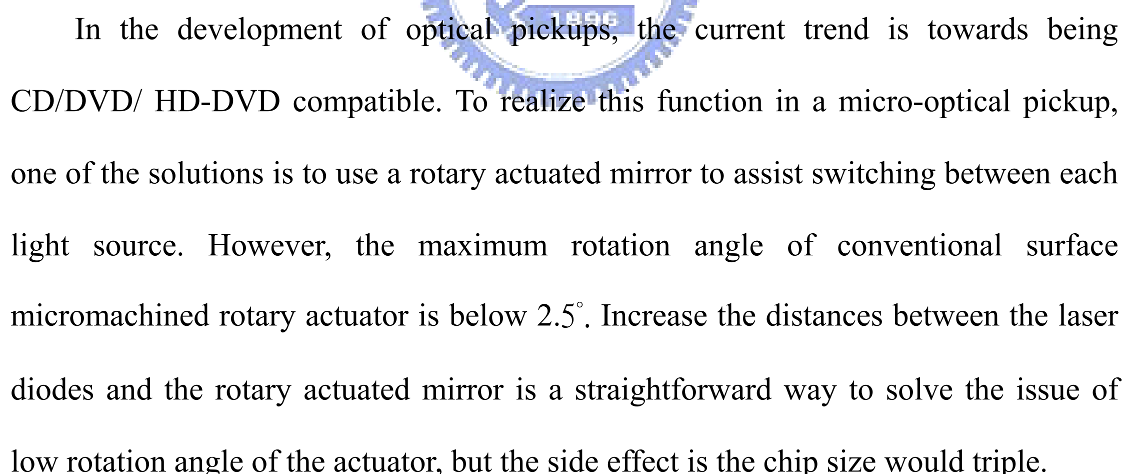

7.1.3 Micro Reflective System

In the development of optical pickups, the current trend is towards being CD/DVD/ HD-DVD compatible. To realize this function in a micro-optical pickup, one of the solutions is to use a rotary actuated mirror to assist switching between each light source. However, the maximum rotation angle of conventional surface micromachined rotary actuator is below 2.5°. Increase the distances between the laser diodes and the rotary actuated mirror is a straightforward way to solve the issue of low rotation angle of the actuator, but the side effect is the chip size would triple.

Using a parabolic mirror and a prism, the micro reflective system, which reflects the incident beam to large angle under constant air gap and fixed reflection point, has been demonstrated. The maximum equivalent scan angle is 38°, which is almost three times larger as compared with that of conventional micro rotary mirror. The concept can be applied in a surface micro-machined pickup to realize a CD/DVD/HD-DVD

compatible system by replacing the prism and the parabolic reflector with a set of mirrors and a vertical parabolic reflector, respectively.

7.2 Future works

The proposed microoptical components, the switchable grating, the polarized beam splitter, and the micro reflective system, successfully demonstrated to enhance the function of micro-optical pickups. Their applications may not only be limited to the micro-optical pickup systems. For example, the switchable grating can be applied in the optical communication as a dynamic beam steering device. Polarized beam splitters can combine with actuators as an array of filters for optical signal processing.

In this dissertation, although the novel functions of the devices were demonstrated, the realization of a commercial micro-optical pickup is still limited by the following challenges:

(a) ***Efficiency:*** The optical efficiency of each element is limited to the available quantized levels and minimum line-width. The total efficiency of the pickup is also significantly reduced as the number of elements increases. To enhance efficiency, a finite conjugate system with fewer optical elements should be adopted.

(b) ***Material:*** The optical performance suffers from high curvature of the polysilicon frame and the optical film itself due to the residual stress. This issue can be solved by using a thicker and stress-less single crystal silicon film to replace the poly-silicon film.

(c) ***Release:*** HF solution is used to remove the silicon-dioxide sacrificial layer. However, it also damages the silicon nitride optical layer. The solution of this process issue depends on a more smart design of the pickup by reducing the

contact time of the optical film with HF solution during the release step.

(d) ***Objective lens:*** To fabricate a SiN diffractive element with NA> 0.5 requires a minimum line-width of 0.3 μm. This is beyond the capability of current etching tool. Besides the optical performance of aspherical surfaces in both sides of the objective lens can't be fully realized using a single diffractive element, which also induces optical aberration.

To cover these challenges, a finite conjugate system based micro optical pickup is proposed. It combines the advantages of the simple fabrication of the stacked type pickup and the design flexibility of the surface micro-machined type pickup. The structure is consisted of one glass, two general wafers, and one silicon on insulator wafer (SOI). The optical devices include a laser diode, a photo diode, a 45° upward beam splitter, a hologram, and an refractive objective lens, as shown in Fig. 7-1(a).

In the forward optical path, the beam splitter can be used to direct the incident light to the objective lens and the disc. In the backward optical path, the beam splitter is tranmissive. The HOE is used to produce asymetrical spot on the photo diode, which monitors the focusing status of the disc. As compared with a conventional optical pickup, the required optical elements are significantly reduced. Besides, the HOE is realized on a flat wafer with its back side being etched using the bulk etching, so no HF release procedure is required. The beam splitter is composed of a silicon nitride film mounted on a single-crystal silicon frame to reduce the curvature. The specification obtained from ZEMAX is shown in Fig. 7-1(b). The simulation value shows the dimension of the pickup is feasible using the current fabrication tools. The tolerance tilt of the 45° upward beam splitter is 0.08°, which is achievable using stacked bonding technology.

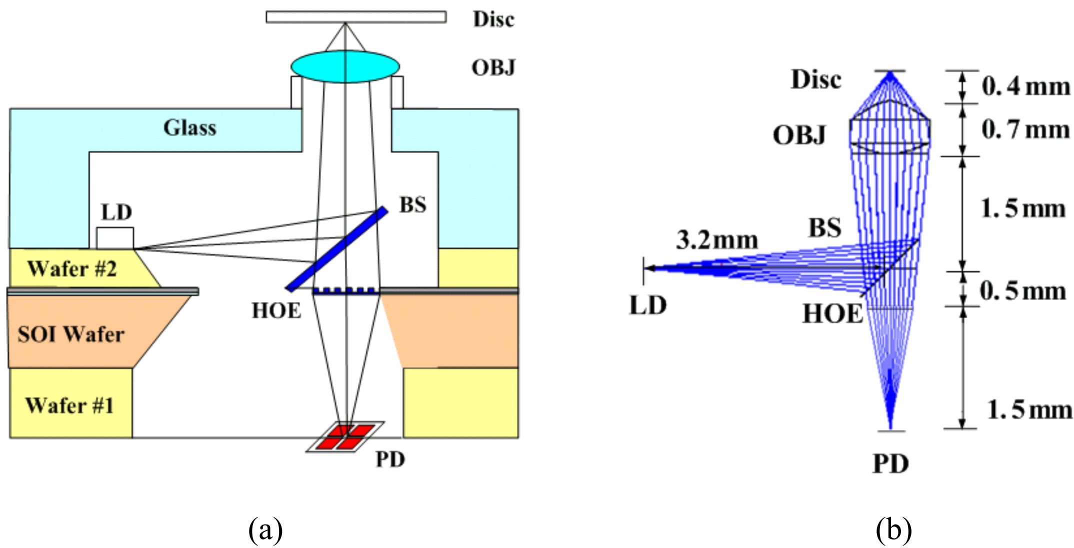

(a) (b)

Fig 7-1. A surface-micromachined optical pickup based on the finite conjugate design (a) and its specification according to ZEMAX (b).

The features of the new design include:

(a) **45° upward beam splitter**, which is used to replace the beam splitter and the 45° upward mirror in the previous design. In this way, the optical elements can be reduced.

(b) **5-μm silicon frame**, which is supplied by a SOI wafer. Since most optical elements are attached within the thick silicon frame, the curvature can be reduced. FEM simulation shows the deformation of the beam splitter with a 500-μm diameter is below $5.6e^{-3}$, as shown in Fig. 7-2.

(c) **No laborious assembly.** Since only the 45° upward beam splitter requires to be assembled, the yield of the new design can be enhanced as compared with the previous design.

(d) **Smart mask design.** There are no etch holes and dimples in the optical pattern, which induces no optical noise. To help release, a back side bulk etching is designed. All etch holes are defined in the side latches as shown in Fig. 7-3.

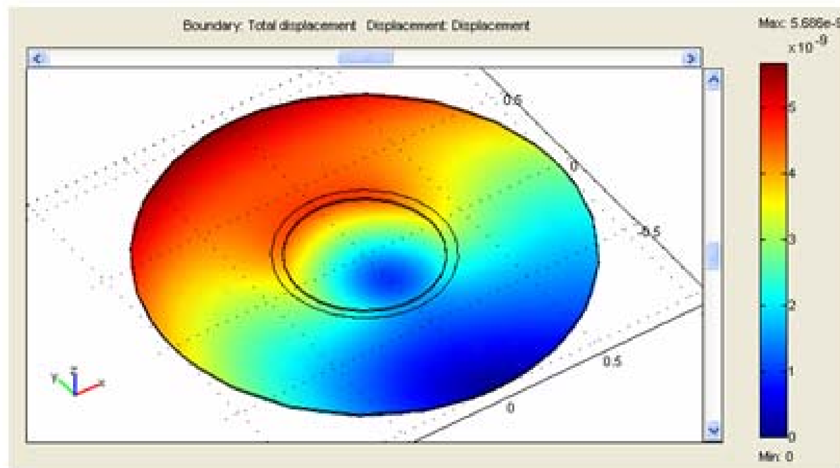

Fig 7-2. FEM shows the deformation of the beam splitter is below 5.6e^{-3}.

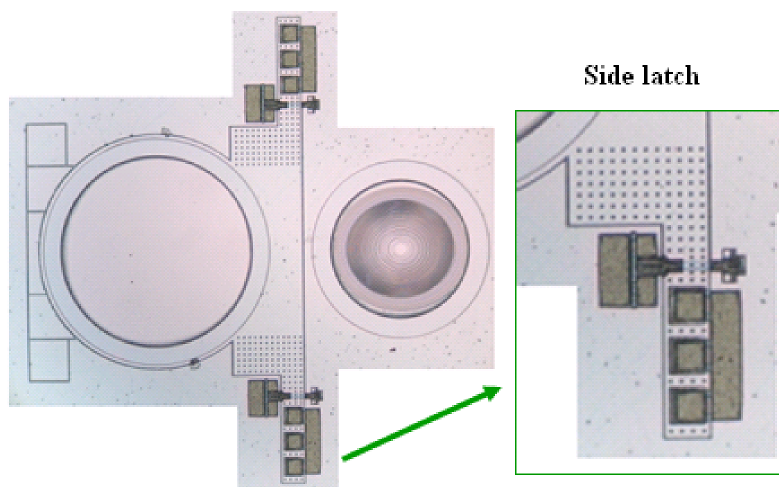

Fig 7-3. Photograph of the smart mask design. The etch holes concentrate on the side latches.

(e) **Astigmatic HOE.** A hologram element (HOE) is used to monitor the working distance between the disc and the objective lens. It is based on a 4-phase levels design, as shown in Fig. 7-4.

(f) **Reasonable S-curve.** ZEMAX simulation in Fig. 7-5 shows the linear range of the focus error signal (S-curve) is 11 μm, which is comparable with that of the current commercial optical pickups.

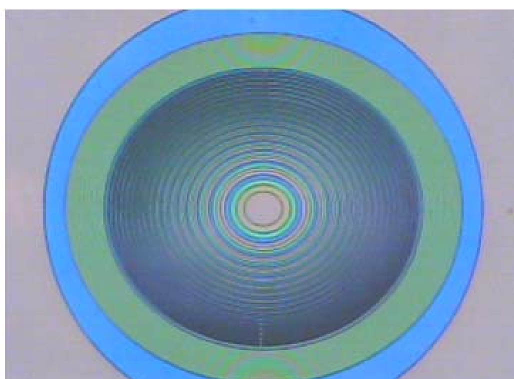

Fig 7-4. Photograph of the 4-phase levels HOE.

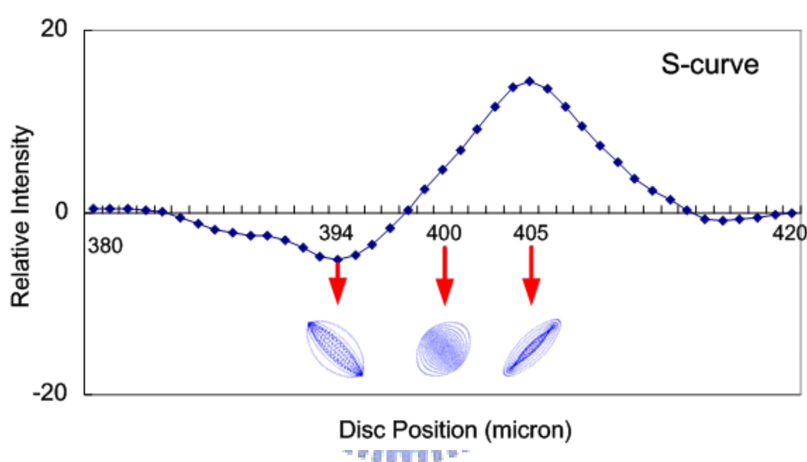

Fig 7-5. Simulation result of focus error signal.

For future works, in the short term the HOE and BS in SOI wafer and the laser diode bonding on wafer#2 can be integrated together to demonstrate its optical performance. In the long term, this work can be further incorporated with the previous developed devices to realize a multifunctional commercial micro-pickup as shown in Fig. 7-6. It is a finite-conjugate optical reading/writing system including a semiconductor laser diode (LD), a photodetector, a switchable grating, a 3 layered stacked-film beam splitter, a hlographic optical element (HOE), and an objective lens. The switchable grating is added to produce a single beam state and a multiple beams

state.

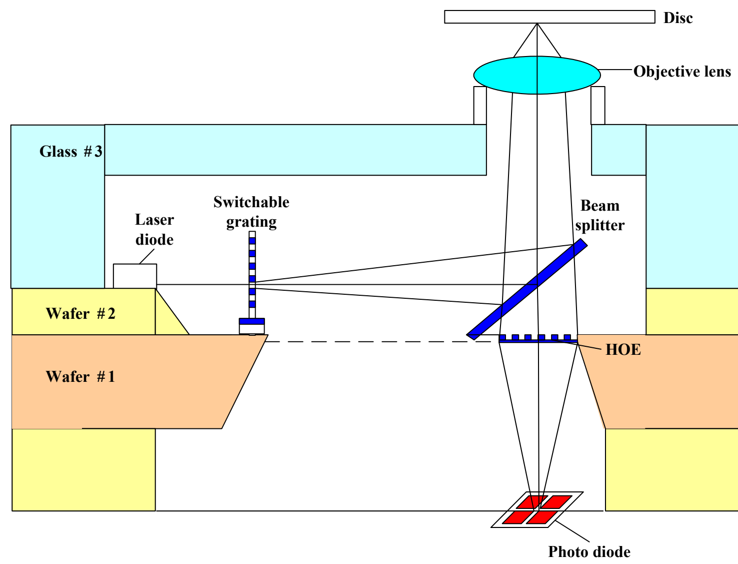

Fig 7-6. A surface-micromachined optical pickup based on the finite conjugate design.

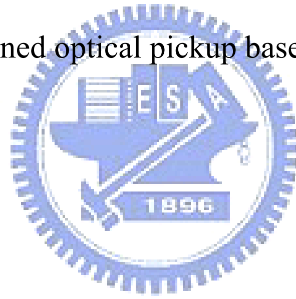

Reference

[1] S. Ura, T. Suhara, H. Nishihara and J. Koyama, *J. Lightw. Technol.***7**, p. 913 (1986).

[2] T. Shiono and H. Ogawa, *Appl. Opt*. **33**, p. 7350 (1994).

[3] Jenq-Yang Chang, Chih-Ming Wang, Chien-Chieh Lee, His-Fu Shih, and Mount-Learn Wu, *IEEE Photon. Teahnol. Lett.* **17**, p. 214 (2005).

[4] L.Y. Lin, J. L. Shen, S. S. Lee, and M. C. Wu, *Opt. Lett*.**21**, p. 155 (1996).

[5] A. Alon and J. Finkelstein: World Patent WO 98/37554 (1998).

[6] A. Alon and T. Kosoburd: U.S. Patent. No. 6,411,573 (2002).

[7] R. Katayama, K. Yoshihara, Y. Yamanaka, M. Tsunekane, K. Kayanuma, T. Iwanaga, O. Okada, and Y. Ono, *Jpn. J. Appl. Phys.*, Part 1 **31**~2B, p. 630 (1992).

[8] H. Okumura, K. Arai, N. Kawamura, H. Tokumaru, and H. Okuda, *Proc. SPIE* **4090**, p. 329 (2000).

[9] Hsi-Fu Shih, *Jpn. J. Appl. Phys.*,**44**~4A, p. 1815 (2005).

[10] L.Y. Lin, S. S. Lee, K. S. A. Pister, and M. C. Wu, *Appl. Phys. Letter*. **66**, p. 2946 (1995).

[11] K. S. J. Pister, M. W. Judy and S.R. Burgett and R. S. Fearing, *Sensors and Actuator*s *A* **33**, p. 249 (1992).

[12] S. S. Lee, L.Y. Lin, and M. C. Wu, *Appl. Phys. Letter*. **67**, p. 2135 (1995).

[13] M. E. Motmedi, M. P. Griswold, and R. E. Knowleden, *Proc. SPIE* **1544,** p. 22 (1991).

[14] K. Rastani, A. Marrakchi, S. F. Habiby, W. M. Hubbard, H. Gilchrist, and R. E. Nahory, *Appl. Opt.* **30,** p. 1347 (1991).

[15] M. E. Motamedi, M. C. Wu, and K. S. J. Pister, *Opt. Eng.* **36**, p. 1282 (1997).

[16] A. J. Stevens, W. J. Hossack, and S.Samus, *Appl. Opt.* **34**, p. 190 (1995).

[17] D. A. Pommet, M. G. Moharam, and E. B. Grann, *J. Opt. Soc. Am. A.* **11**, p. 1827 (1994).

[18] J. N. Mait, *J. Opt. Soc. Am. A.* **12**, p. 2145 (1995).

[19] U. Krackhardt, N. Streibl and J. Schwider, *Optik* **95**, p. 137 (1994).

[20] J. A. Cox, T. Werner, J. Lee, B. Fritz and J. Bergstorm, *Proc. SPIE* **1211**, p. 116 (1990).

[21] J. A. Cox, B. Fritz and T. Werner, *Proc. SPIE* **1555**, p. 80 (1991).

[22] W.-H. Lee, *Appl. Opt.* **18**, p. 2152 (1979).

[23] M. T. Ching, R. A. Brennen, and R. M. White, *Proc. SPIE* **1992**, p. 40 (1993).

[24] M. H. Kiang, O. Solgaard, R. S. Muller, and K. Lau, *IEEE Photon. Technol. Lett.* **8**, p1707 (1996).

[25] M. M. Daneman, N. C. Tien, O. Solgaard, A. P. Pisano, K. Y. Lau, and R. S. Muller, *J. Microelectromech. Syst.,* **5**, p159 (1996).

[26] M. J. Daneman, O. Solgaard, N. C. Tien, K. Y. Lau, and R. S. Muller, *IEEE Photon. Technol. Lett.,* **8**, p. 396 (1996).

[27] J. H. Comtois, V. M. Bright, and M. W. Phipps, *Proc.SPIE,* **2642,** p. 10 (1995)

[28] J. H. Comtois and V. M. Bright, *Sens. Actuators A,* **A58**, p. 19 (1997).

[29] T. Akiyama and K. Shono, *J. Microelectromech. Syst.,* **2,** p. 106 (1993).

[30] T. Akiyama, D. Collard, and H. Fujita, *J. Microelectromech. Syst.,* **6**, p. 10 (1997).

[31] S. S. Lee, E. Motamedi, and M. C. Wu, *Proc. 1997 Int. Conf. Solid-State Sensors and Actuators*, paper **1A4.07P** (1997).

[32] G. D. Su, L. Y. Lin, and M. C. Wu, *Proc. Conf. Lasers and Electro-Optics (CLEO),* paper **CWL2** (1997).

[33] Chan E K and Dutton R W, *Proc. SPIE Symposium on the Design and Test of MEMS/MOEMS Devices (Paris)* **3680,** p. 120 (1999)

[34] Rosa M A, Bruyker D D, Volkel A R, Peeters E and Dunec J, *J. Micromech. Microeng.* **14, p.** 446 (2004).

[35] J C Chiou and Y J Lin, *J. Micromech. Microeng.* **15**, p. 1641 (2005)

[36] R. T. Chen, H. Nguyen and M. C. Wu, *Proc. IEEE MEMS'99*, p. 424 (1999).

[37] Http://www.memsrus.com/nc-mumps.poly.html, POLYMUMPS Hankbook.

[38] N. Tas, T. Sonnenberg, H. Jansen, R. Legtenberg and M. Elwenspoek, *J. Micromech. Microeng.* **6,** p. 385 (1996).

[39] R. Maboudian and R. T. Howe: *J. Vac. Sci. Technol.* **B 15,** p. 1 (1997).

[40] C. H. Mastrangelo, and C. H. Hsu, *IEEE/ASME J. of Microelectromechanical Syst.*, **2**, p. 33 (1993).

[41] K. F. Harsh, "Dealing with MEMS stiction and other sticting problems", http://mems.colorado.edu/.

[42] G. T. Mulhern, D. S. Soane, and R. T. Howe, *The 7th Int. Conf. on Solid-State Sensors and Actuators (Transducers **93**)*, p. 296 (1993).

[43] M. Offenberg, B. Elsner and F. Larmer: Ext. Abstr. Electrochemical Soc. Fall Meet., p. 1056, (1994).

[44] Y. I. Lee, K. H. Park, J. H. Lee, C. S. Lee, H. J. Yoo, C. J. Kim and Y. S. Yoon: J. *MEMS* **6**, p. 226 (1997).

[45] C. R. Helms and D. E. Deal: *J. Vac. Sci. Technol.* **A 10**, p. 806 (1992).

[46] C. Pu, Z. Zhu, and Y. H. Lo, *IEEE/Photon. Technol. Lett.* **10**, p. 988 (1998).

[47] Schuegraf, Klaus K. ed, *Thin Film Deposition Process and Techniques* Noyes Publications, Park Ridge, NJ (1988).

[48] Pochi Yeh, *Optical waves in layered media,*Wiley, Singapore (1991).

[49] K.Cheng, *Field and Wave Electromagnetics,* Addison-Wesley, Massachusetts (1989)

[50] Bahaa E. A. Saleh and Malvin Carl Teich, *Fundamentals of photonics,* WILEY-VCH, New York *(1991).*

[51] M. Born, and E. Wolf, *Principle of Optics*, Pergamon Press, New York (1998).

[52] S. Huard, *Polarization of light,* John Wiley & Sons, Chichester (1997)

[53] Schuegraf, Klaus K. ed, *Thin Film Deposition Process and Techniques* , Noyes Publications, Park Ridge, NJ (1988).

[54] Wolf S and Tauber R, *Silicon Processing for the VLSI Era, Vol. 1: Process Technology* , Lattice, Sunset Beach, CA (1986).

[55] M. Sekimoto, H. Yoshihara, and T. Ohkubo, *J. Vac. Sci. Technol.* **21,** p. 1017 (1982).

[56] J. G. E. Gardeniers, H. A. C. Tilmans and C. C. G. Visser, *J. Vac. Sci. Technol.* A, **14,**

p. 2879 (1996).

[57] D. Maier-Schneider, A. Ersoy, J. Maibach, D. Schneider, and E. Obermeier, *Sens. Materials*, **7,** p. 121 (1995).

[58] Chao-His Chi, Monolithic MEMS-Based Wavelength-Selective Switches and Cross Connects, Ph.D. Thesis, University of California Los Angeles, 2006.

Publication List

Journal Papers

1. **Chi-Hung Lee**, Yi Chiu, and Han-Ping D. Shieh, “High-extinction-ratio micro polarizing beam splitter for short wavelength optical storage applications”, Optics Express, Vol. 13 (2005), pp. 10292-10301.

2. **Chi-Hung Lee**, Yi Chiu, and Han-Ping D. Shieh, “Micro actuated grating for multi-beam optical pickups”, Optics Express, Vol. 15 (2007), pp. 1408-1414.

3. **Chi-Hung Lee**, Yi Chiu, and Han-Ping D. Shieh, “Binary Phase Micro-Grating and Polarization Beam Splitter for Free-Space Micro Optical Pickups”, Optical. Eng., Vol. 46 (2007), issue 8.

4. **Chi-Hung Lee**, Yi Chiu, Sagi Mathai, M. C. Tien, M. C. Wu, and Han-Ping D. Shieh, "A Planar Micro-reflective System with Enhanced Angular Deflection for Silicon-based Planar Lightwave Circuits", Japanese Journal of Applied Physics, Accepted on June 20 (2007).

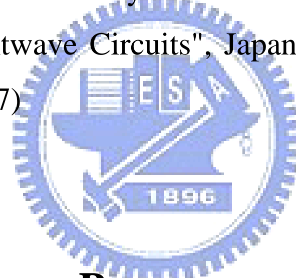

International Conference Papers

1. **Chi-Hung Lee,** Yi Chiu, an d Han-Ping D. Shieh, “Micro polarizing beam splitter for Blue Wavelength Optical Pickups Application”, Finland, IEEE/LEOS, Optical MEMS 2005., Paper number E5.
2. Chao-Hsi Chi, Chenlu Hou**, Chi-Hung Lee,** “Silicon-based on-chip micromirrors for DWDM wavelength-selective”, USA, IEEE/LEOS Optical MEMS 2006, Paper number P27.

Domestic Conference Paper

1. Chi-Hung Lee, Yi Chiu, an d Han-Ping D. Shieh, “Micro-grating for free-space micro optical pickup” Optics and Photonics Taiwan’04.

2. Wang-Ling Tsai, Chi-Hung Lee, Chung-hao Tien, Yi Chiu, an d Han-Ping D.

Shieh, “The polarization beam splitter for micro-optical pickup” Optics and Photonics Taiwan’04.

3. Chi-Hung Lee, Yi Chiu, an d Han-Ping D. Shieh, “Micro actuated grating for multi-beam optical pickups” Optics and Photonics Taiwan’06.

Cited by International Magazine

1. John Wallace, “OPTICAL STORAGE: Miniature optical pickup has dual-suspended-film beamsplitter” Laser Focus World, (Feb. 2006)

Patents

1. 李企桓，李志宏，黃啟業，周良奎 “化學機械研磨台”，（中華民國專利公告號00536448）

2. 李企桓，李志宏，黃啟業，周良奎 “輔助研磨裝置”，（中華民國專利公告號 00508286）

Pending:

1. 李企桓, 邱一, 謝漢萍, "可切換單光束與多光束之微型光學讀寫頭", (中華民國專利申請中）

Awards

2003 – 交大資格考筆試第一名

2004 – 台灣光電科技研討會(OPT’04)優良學生論文獎.

2005 – 獲選國科會千里馬計畫獎學金一年（留學加州大學柏克萊分校）

Vita

Name: Chi-hung Lee 李企桓

Day of birth: Jan. 12 1974

Address: 台南縣學甲鎮宅港里 33 號

Education

Sep. 02' – Presnt : National Chiao Tung University, Hsinchu, Taiwan. Ph. D. in Institute of Electro-Optical Engineering.

Sep. 95' – Jun. 97' : National Taiwan University, Taipei, Taiwan. Master in Materials Science and Engineering.

Sep. 91' – Jun. 95' : National Cheng-Kung University, Tainan, Taiwan. Bachelor in Materials Science and Engineering.

Experience

May. 99' – Sep. 02' : CMP Process Engineer, Winbond Co., Hsin-Chu, Taiwan.

Sep. 05' – Sep. 06': Visiting scholar at the EECS, University of California, Berkeley, California, U.S